Heinz-Siegfried Kitzerow   Christian Bahr
Editors

Chirality in
Liquid Crystals

Foreword by Sivaramakrishna Chandrasekhar

With 326 Illustrations

Springer

Heinz-Siegfried Kitzerow
Department of Chemistry
University of Paderborn
Warburger Strasse 100
D-33098 Paderborn
Germany
kitzerow@chemie.uni-paderborn.de

Christian Bahr
Institute of Physical Chemistry
University of Marburg
Hans-Meerwein-Strasse
D-35032 Marburg
Germany
bahr@mailer.uni-marburg.de

This book is dedicated to Prof. Gerd Heppke
with respect and kind regards.

5
Cholesteric Liquid Crystals: Defects and Topology

O.D. LAVRENTOVICH AND M. KLEMAN

This chapter reviews the basic static properties of defects in cholesteric liquid crystals. The elastic features of the cholesteric phase with deformations at short-range and long-range (as compared to the cholesteric pitch) scales are discussed. Spatial confinement, together with the relative smallness of the twist elastic constant, often leads to twisted and thus optically active structures even when the liquid crystal is composed of nonchiral molecules. The application of topological methods is illustrated using the models of twisted strips, closed DNA molecules, and defect lines—disclinations and dislocations. The homotopy classification of defects in cholesterics is similar to that in biaxial nematics, and predicts phenomena such as the topological entanglement of disclinations and the formation of nonsingular soliton configurations. The spatial confinement of ordered structures (represented, for example, by cholesteric droplets suspended in an isotropic matrix) imposes certain restrictions on the configurations of the order parameter and requires the appearance of topological defects in the ground state. The layered structure of cholesterics leads to the formation of large-scale defects such as focal conic domains and oily streaks.

5.1   Introduction

Chiral liquid crystals belong to a wide class of soft condensed phases. The director field in the ground state of chiral phases is nonuniform because molecular interactions lack inversion symmetry. Among the broad variety of spatially distorted structures the simplest one is the cholesteric phase in which the director n is twisted into a helix. The spatial scale of background deformations, e.g., the pitch p of the helix, is normally much larger than the molecular size ($p \geq 0.1$ μm) since the interactions that break the inversion symmetry are weak.

The twisted ground state of chiral liquid crystals willingly accepts the additional deformations imposed by external fields, surface interactions, or by a tendency of molecules to form smectic layers, hexagonal order, or double-twist arrangements. Very often such additional deformations result in topo-

logical defects. The complexity of twisted structures with defects makes the cholesteric liquid crystals an important subject to test the modern concepts of relationship between the symmetry of molecular interactions and macromolecular organization. The connection between symmetry and defects has been for decades at the very heart of physics [1]–[3]; nowadays, it becomes the subject of studies in biology.

In this chapter we discuss the basic features of deformed structures in liquid crystals with chiral order. The characteristic scale of these deformations has to be compared to the scale p of ground deformations. Properties of defects and deformations that occur at scales smaller and larger than p are quite different.

We start this chapter with a brief introduction to the elastic theory of cholesteric phases with the object of clarifying the difference in description of short- and long-range deformations (Section 5.2). Section 5.3 discusses "weak" twist deformations. Weak twist deformations are not necessarily caused by the chiral nature of the liquid crystal molecules. The recent discovery [4] of chiral domains in smectics composed of achiral molecules confirms the general thesis that chirality in soft-matter systems does not always require chiral centers in the molecules, see the paper by G. Heppke and D. Moro [5]. Examples of chiral bulk deformations can be seen even in much simpler nematic samples, where the symmetry is broken either because of the explicit action of the boundary conditions or because of a more subtle mechanism that involves the smallness of the twist elastic constant K_2. Section 5.4 explains the elementary topological concepts employing a model of twisted strips; related to these strips are closed DNA molecules. The homotopy classification of line defects, disclinations, and dislocations, and its predictions (such as the topological entanglement of lines) are presented in Section 5.5. Homotopy theory defines the necessary conditions for the formation of defects by deducing the classes of possible defects from the symmetry group of the order parameter. Sufficient conditions are often provided by the spatial boundedness of the ordered media. In Section 5.6 we describe how the spatial confinement of an ordered system leads to the appearance of defects in its equilibrium state. Section 5.7 reviews the topological solitons (or "textures") which are topologically stable but nonsingular. Section 5.8 discusses defects such as focal conic domains and the oily streaks provoked by the tendency of cholesteric layers to keep an equidistance in large-scale deformations. Finally, Section 5.9 is an look forward to possible further studies in the field of defects in chiral liquid crystals.

5.2 Elastic Theory and the Hierarchy of Scales

We deal with situations where the director field deviates from the ideal helix. There are two complementary approaches to describe distortions in the cholesteric phase, depending on the ratio L/p, where L is the characteristic

scale of the deformations or the size of the liquid crystal sample. We distinguish weakly twisted cholesterics ($L/p \ll 1$) and strongly twisted ($L/p \gg 1$) cholesterics.

5.2.1 Weakly Twisted Cholesterics

In the absence of external fields or bounding surfaces, the equilibrium director configuration of the uniaxial cholesteric phase has the form

$$\mathbf{n}(\mathbf{r}) = \mathbf{u}\cos\varphi(\mathbf{r}) + \mathbf{v}\sin\varphi(\mathbf{r}). \tag{5.1}$$

Here $\mathbf{u}$ and $\mathbf{v}$ are two mutually perpendicular unit vectors (with constant orientation in space) and

$$\varphi(\mathbf{r}) = q_0\boldsymbol{\chi}\mathbf{r} + \text{const}, \tag{5.2}$$

where $q_0 = 2\pi/p$ and $\boldsymbol{\chi} = \mathbf{u} \times \mathbf{v}$ is a unit vector along the helix axis [1]–[3]. The twisted configuration (5.1) minimizes the free elastic energy density

$$f = \tfrac{1}{2}K_1(\text{div}\,\mathbf{n})^2 + \tfrac{1}{2}K_2(\mathbf{n}\cdot\text{curl}\,\mathbf{n} + q_0)^2 + \tfrac{1}{2}K_3(\mathbf{n} \times \text{curl}\,\mathbf{n})^2, \tag{5.3}$$

with splay (K_1), twist (K_2), and bend (K_3) terms; q_0 is positive for a right-handed cholesteric, and negative for a left-handed cholesteric provided the trihedron $(\mathbf{u},\mathbf{v},\boldsymbol{\chi})$ forms a right-handed coordinate system. For example, $(n_x, n_y, n_z) = (\cos q_0 z, \sin q_0 z, 0)$ yields $f = 0$ in the Cartesian coordinate frame for both $q_0 > 0$ and $q_0 < 0$.

Expression (5.3) contains only the first derivatives of the director. Since f is quadratic in $n_{i,j}$, $f \sim (n_{k,j})^2$, the *second* derivatives $n_{i,jk}$ might bring comparable contributions to f. Invariant terms involving second derivatives are usually written as the sum of the mixed splay-bend (K_{13}) and saddle-splay (K_{24}) terms:

$$f_{13} + f_{24} = K_{13}\,\text{div}(\mathbf{n}\,\text{div}\,\mathbf{n}) - K_{24}\,\text{div}(\mathbf{n}\,\text{div}\,\mathbf{n} + \mathbf{n} \times \text{curl}\,\mathbf{n}). \tag{5.4}$$

Although it is not difficult to see that the saddle-splay term can be reexpressed as a quadratic form of the first derivatives, $\text{div}(\mathbf{n}\,\text{div}\,\mathbf{n} + \mathbf{n} \times \text{curl}\,\mathbf{n}) = n_{i,i}n_{j,j} - n_{i,j}n_{j,i}$, we will keep the form (5.4) for subsequent discussion. The divergence nature of the terms (5.4) allows us to transform the volume integral $\int(f_{13} + f_{24})\,dV$ into a *surface* integral by virtue of the Gauss theorem

$$\int \text{div}\,\mathbf{g}\,dV = \oiint_A \mathbf{v} \cdot \mathbf{g}\,dA, \tag{5.5}$$

where $\mathbf{g} = (K_{13} - K_{24})\mathbf{n}\,\text{div}\,\mathbf{n} - K_{24}\mathbf{n} \times \text{curl}\,\mathbf{n}$ and $\mathbf{v}$ is the unit vector of the outer normal to the surface A. However, K_{13} and K_{24} must not be neglected on the grounds of transformation (5.5). Whatever the way of integration of f, f_{13}, and f_{24}, the resulting elastic energy scales linearly with the size of the deformed system. The difference between f and $(f_{13} + f_{24})$ is more subtle and shows up when one looks for an equilibrium director configuration by min-

imizing the total free-energy functional $\int (f + f_{13} + f_{24})\,dV$: the K_{13} and K_{24} terms do not alter the Euler–Lagrange variational derivative for the bulk, but they can influence the equilibrium director through the boundary conditions at the surface A (which might also be the imaginary surface of the defect cores). Since the procedure of inclusion of the K_{13} term into the minimization problem is still debated, we will not consider this term here. The K_{24} term will be preserved since it brings an important insight into the nature of some chiral structures, such as double-twist configurations.

When $L/p \ll 1$, the cholesteric does not differ much from the nematic phase. No wonder therefore that optical observations for weakly twisted cholesterics reveal "thick" (nonsingular) and "thin" (singular) line defects —disclinations similar to that in the nematic phase. Moreover, in droplets of the so-called "compensated" cholesteric mixtures with extremely small L/p one can observe point defects [6] which, from the topological point of view, are allowed only in a nematic phase.

The behavior of weakly twisted structures depends on the relative values of the elastic constants in (5.3) and (5.4). As we shall see in the next section, splay and bend distortions are often relaxed by twist. It is therefore important to know the elastic constants for different types of deformations; these constants are specified by molecular structures and interactions.

Small Molecules Liquid Crystals (SMLC's). In most cases, K_2 is small as compared to K_1 and K_3. For example, for 5CB [7]:

$$K_1 = 0.64 \times 10^{-6}\,\text{dyn}, \qquad K_2 = 0.3 \times 10^{-6}\,\text{dyn}, \qquad K_3 = 1 \times 10^{-6}\,\text{dyn}.$$

The coefficient K_{24} is very hard to determine; recent studies reviewed by Crawford and Zumer [8] indicate that in nematics $K_{24} \sim K_1, K_3$.

Liquid Crystal Polymers (LCP) [9]. One does not find in this case the simplicity of SMLCs but, on the other hand, one expects that the coefficients would relate in an interesting way to *molecular conformations*—a field of research which is still open to investigation. A general result is that K_2 remains smaller than K_1 and K_3, and is of the same order of magnitude as SMLCs. This result is rather intuitive, since the molecular length does not play a priori an important role in a pure twist deformation. On the other hand, K_1 and K_3 are strongly modified. In rigid polymers, K_1 and K_3 increase with molecular weight and K_3 increases faster than K_1. In semiflexible polymers, two features appear when the molecular weight increases. First, the molecular length l becomes larger than the *persistence length* Λ; this has an effect on K_3, whose variation with l reaches a maximum when $l > \Lambda$. Second, the density of *chain-ends* decreases when l increases; this has a direct effect on K_1. In the limit when the chains become infinitely long, any splay deformation at constant polymer density is forbidden, and K_1 becomes increasingly large. The chain ends contribute to the total energy by the elastic deformation they carry and by their entropy that gives rise to a large contribution to K_1.

5.2.2 Strongly Twisted Cholesterics

At $L/p \gg 1$, the elastic properties of the cholesteric are close to that of the lamellar phases. Here again, two different situations are possible. First, the cholesteric layers might be only slightly bent and preserve the topology of flat surfaces. These small deformations can be described by a single scalar variable, the component of the displacement $u(x, y, z)$ of the layers along the normal of the nonperturbed layers, taken as the z-axis. The free-energy density in terms of the layer dilatation and small tilts is [1]–[3]:

$$f = \tfrac{1}{2}B\left(\frac{\partial u}{\partial z}\right)^2 + \tfrac{1}{2}K\left(\frac{\partial^2 u}{\partial x^2} + \frac{\partial^2 u}{\partial y^2}\right)^2, \tag{5.6}$$

where one introduces renormalized constants $B = K_2 q_0^2$ and $K = \tfrac{3}{8}K_3$; note that this renormalization does not take into account divergence terms.

When the deviations of layers from the flat geometry are substantial, the deformations are more appropriately characterized by the principal curvatures $\sigma_1 = 1/R_1$ and $\sigma_2 = 1/R_2$ of the cholesteric layers [10]. The elastic free energy density can be cast in the form

$$f = \tfrac{1}{2}K(\sigma_1 + \sigma_2)^2 + \tfrac{1}{2}B\gamma^2, \tag{5.7}$$

where $\gamma = |p - p_0|/p_0$ is a relative dilatation of the layers. Scaling arguments show that the curvature elasticity $f_c = \tfrac{1}{2}K(\sigma_1 + \sigma_2)^2$ and the "positional" elasticity $f_p = \tfrac{1}{2}B\gamma^2$ should be treated on different footings when $L/p \gg 1$. Let L be a typical length of the deformation that shows up in all three spatial directions. The corresponding energies are

$$F_c \sim KL \qquad \text{and} \qquad F_p \sim BL^3; \tag{5.8}$$

hence $F_p/F_c \sim (L/p)^2 \gg 1$. In other words, at $L/p \gg 1$, the theory treats the cholesteric medium as a system of equidistant (and thus parallel) layers with predominantly curvature distortions. Generally, the boundary conditions can be satisfied only by the appearance of large-scale defects, such as *focal conic domains* and *oily streaks*.

The coarse-grain model (5.7) does not take into account the saddle-splay term $f_{ss} = \bar{K}\sigma_1\sigma_2$, where $G = \sigma_1\sigma_2$ is the Gaussian curvature of layers, and $\bar{K}$ is the saddle-splay constant (*different* from K_{24} in (5.4)). The dependence of $\bar{K}$ on the Frank constants has not been calculated so far. Partially, the omission is justified by the fact that the $\bar{K}$ term does not change when the layers experience *small* fluctuations around the basic topologies (flat layers, cylinders, tori, etc.). Transitions between these geometries, such as nucleation of a focal conic domain in a system of flat layers, should involve the $\bar{K}$ term. According to the Gauss–Bonnet theorem, the integral of the Gaussian curvature over a closed manifold is a constant defined by the *Euler characteristic E* of the manifold

$$\oint \sigma_1 \sigma_2 \, d\Sigma = 2\pi E; \qquad (5.9)$$

$E = 0$ for a torus and $E = 2$ for a sphere. This topological feature makes the Gaussian curvature insensitive to small elastic deformations and sensitive to topological changes. In addition, it is precisely the nonzero value of the integral (5.9) that brings topological defects into the ground state of the confined liquid crystals, such as suspended droplets, as discussed in Section 5.6.

5.3   Weak Twist Deformations

5.3.1   Confinement-Induced Twists

As was established a long time ago by Mauguin [11], pure twist deformations can be produced by placing a nonchiral nematic liquid crystal between two parallel rubbed solid surfaces and then rotating one plate in its own plane relative to the other. Such a structure is optically active despite the fact that the nematic molecules are not chiral. The twist is maintained by the surface "azimuthal" anchoring.

One would expect that when the director is allowed to rotate in the plane of one of the plates (an "isotropic" plate with no azimuthal anchoring), the twist and optical activity would disappear. Surprisingly, this was not what Meyerhofer et al. observed by placing nematic droplets on a rubbed plate and letting the upper surface of the liquid free [12]. The sessile droplets clearly demonstrated significant optical activity, even when there was no external electric or magnetic field. The phenomenon might be explained if one takes into account that the free surface of a sessile drop is usually curved (except in a rare case of complete wetting) and tilted with respect to the horizontal supporting plate. The wedge geometry forces the director to align normally to the thickness gradient (say, along axis y in Figure 5.1) in order to reduce the amount of splay and thus to reduce the elastic energy. The phenomenon can be called a "geometrical anchoring" [13]. However, when the bottom plate is rubbed along any direction different from y, the competition between the two easy axes might result in twist.

To show this, let us calculate the energy per unit area of the wedge, neglecting director distortions in the plane of the cell [13]. We parametrize the director through the polar angle θ and the azimuthal angle φ as $(n_x, n_y, n_z) = (\sin\theta(z)\cos\varphi(z), \sin\theta(z)\sin\varphi(z), \cos\theta(z))$. At the bottom plate, $\theta(z = 0) = \pi/2$ and $\varphi(z = 0) = 0$. The director is tangential to the upper surface. If the two bounding surfaces were parallel, then in equilibrium $\theta(z) = \pi/2$ and $\varphi(z) = 0$. Suppose now that the upper surface is tilted around the y-axis by an angle γ. The polar angle $\theta(z = d)$ now depends on γ and on the azimuthal parameter φ_0 which is the angle between $\mathbf{n}$ and a fixed axis x' in the inclined upper plane: $\theta(z = d) = \arccos(\sin\gamma\cos\varphi_0)$. Small

(a)   (b)
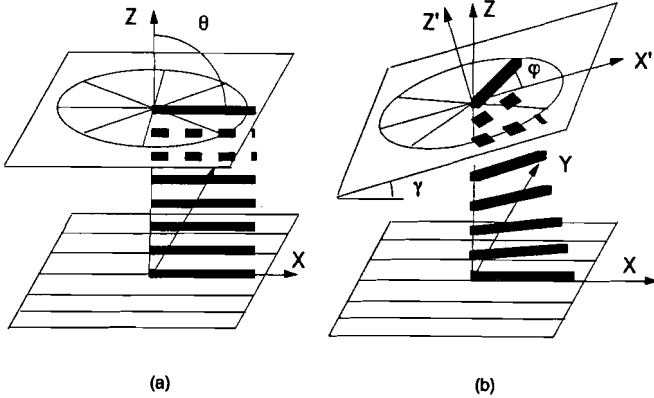
FIGURE 5.1. A tangentially aligned nematic liquid crystal confined between two plates; the bottom plate is rubbed, the top plate is isotropic. The tilt of the upper plate tends to reorient the director normally to the plane of the figure (geometrical anchoring). In combination with surface anchoring at the bottom plate, this results in the twist deformation.

deviations from the uniform state, $\theta(z) \to \pi/2 + \theta_1(z)$ and $\varphi(z) \to 0 + \varphi_1(z)$ lead to the free energy density $f = \frac{1}{2}K_1\theta_{1,z}^2 + \frac{1}{2}K_2\varphi_{1,z}^2$. The bulk equilibrium equations, $\theta_{1,zz} = 0$ and $\varphi_{1,zz} = 0$, together with the boundary conditions above, lead to the energy per unit area

$$F = \frac{K_1}{2d}[\arcsin(\sin\gamma\cos\varphi_0)]^2 + \frac{K_2}{2d}\left[\arctan\left(\frac{\tan\varphi_0}{\cos\gamma}\right)\right]^2. \tag{5.10}$$

According to (5.10), the equilibrium azimuthal angle at the upper surface can be nonzero (Figure 5.2). This implies twist and hence optical activity of the sessile droplet. The twist angle increases as the ratio K_2/K_1 decreases so that the effect might be strongly pronounced for nematic polymers such as poly-γ-benzylglutamate (PBG), where the ratio K_2/K_1 can be as small as 0.1 or even smaller [14].

Twist relaxation of splay and bend is a general phenomenon in materials with small K_2. Chiral structures can occur in defective nematic samples even when there is no azimuthal anchoring at all. Twisted brushes observed by Press and Arrott in textures of lens-shaped nematic droplets floating on the water surface are one example [15]. Another well-known illustration of twist relaxation is the periodic pattern of stripes that occur in the geometry of splay Frederiks transition in polymer nematics with a small (less than 0.33) ratio K_2/K_1 [16]. A field applied normally to the planar nematic cell causes stripe structures composed mostly of twist rather than the uniform splay response observed in regular materials.

An especially clear demonstration of twist relaxation is given by tangentially anchored spherical nematic droplets suspended in an isotropic matrix (glycerin), Figure 5.3. The director lines join two point defects—boojums at
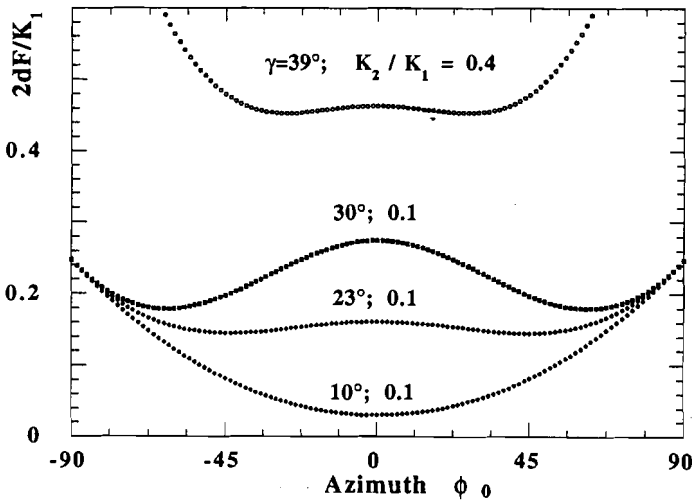
FIGURE 5.2. Elastic energy versus azimuthal angle at the top surface for the nematic wedge, see text. The twist angle increases with the increase in tilt γ and the decrease in the ratio K_2/K_1.

the poles of the droplet. However, instead of a naive picture, with lines being meridians that lie in the planes of constant azimuth, one observes a twisted structure [17]. The director lines are tilted with respect to the meridional planes. This tilt decreases as one approaches the axis of the droplet. As in the previous example, the twist replaces energetically costly splay [18]. Each droplet is optically active despite the nonchiral nature of the molecules of both the nematic and matrix. Of course, there is an equal number of "left"- and "right"-handed droplets in the dispersion.

The droplets shown in Figure 5.3 present in fact a double twist rather than a simple unidirectional twist. Double twist is discussed below in relation to the saddle-splay coefficient.

5.3.2   Double Twist

One may inquire about the meaning of the K_{24} term in a weakly twisted cholesteric; the solution is in the *double-twist* tendency of cholesterics [19]–[21]. Let n_0 be some director, e.g., along the axis Z in Figure 5.4. In the local state of the smallest energy, chiral molecules in the vicinity of n_0 tend to rotate helically along *all* the directions perpendicular to n_0. This double twist is energetically preferable to the one-dimensional twist, at least for some chiral materials.

In cylindrical coordinates, the elementary double-twist configuration is

$$n_r = 0, \qquad n_\theta = -\sin\psi(r), \qquad n_z = \cos\psi(r), \qquad (5.11)$$
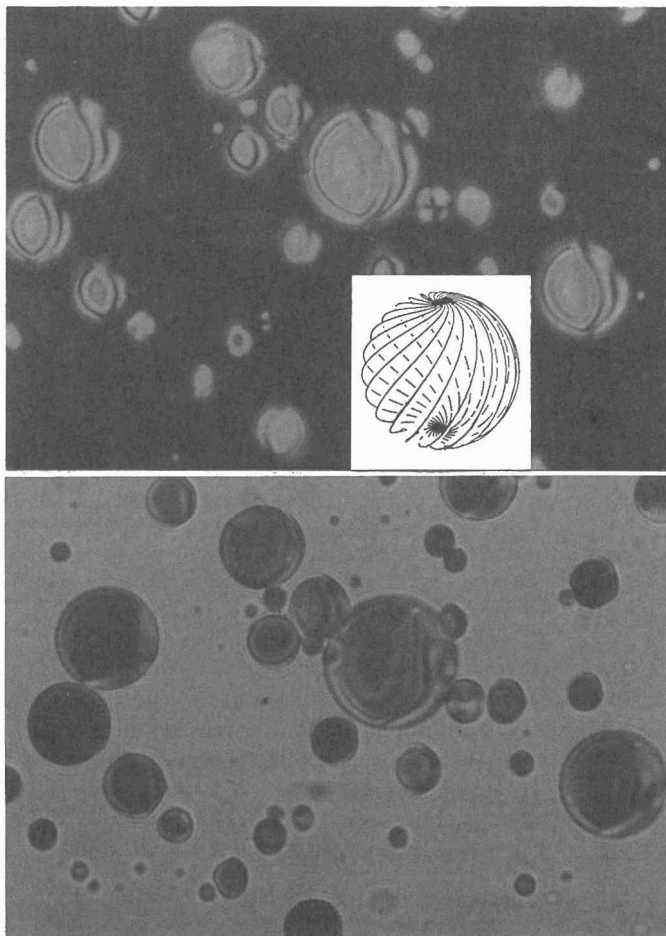
FIGURE 5.3. Double-twisted nematic droplets suspended in an isotropic matrix. The central part of the droplet is bright when the polarizers are crossed and one of them is aligned along the droplets' axes (a); the central part can be made dark by changing the angle between the polarizer and analyzer. This behavior indicates the optical activity of the droplets caused by the director twist. The insert shows the director configuration at the droplet's surface. Nematic n-butoxyphenyl ester of nonylhydrobenzoic acid dispersed in glycerin [17].

with $\psi(0) = 0$. The free energy is

$$f = \tfrac{1}{2} K_2 \left(q_0 - \frac{\partial \psi}{\partial r} - \frac{1}{r} \sin \psi \cos \psi \right)^2 + \tfrac{1}{2} K_3 \frac{\sin^4 \psi}{r^2} - \frac{K_{24}}{r} \frac{d}{dr} (\sin^2 \psi). \quad (5.12)$$

There is no K_{13} term, since $\operatorname{div} \mathbf{n} \equiv 0$. Integrating f we see that the K_{24} term contributes to the energy of a cylinder of matter of radius R by the quantity
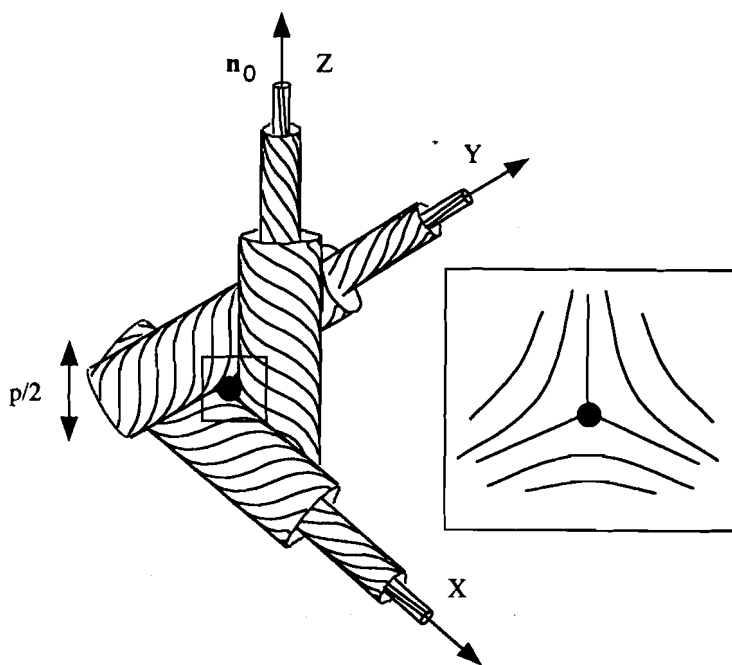
FIGURE 5.4. Blue phases are composed of regions with double twist; three such regions, with a singularity that relieves frustration between them, are shown in the figure. Two cylinders with double twist match at the contact point if the director tilt at their surfaces is $\pi/4$; however, the region where all three cylinders meet is singular. In current models, such singularities form a network of disclination lines. The circle marks the "core" of the disclination; the insert shows the director lines around the core.

$$F_{24} = -K_{24} \int_0^R 2\pi \frac{d}{dr} (\sin^2 \psi) \cdot dr = -2\pi K_{24} \sin^2 \psi(R), \qquad (5.13)$$

which is negative for any value of $\psi(R) \neq \pi n$, when K_{24} is positive. The nucleation of a double-twisted cholesteric geometry is favored in such a case, in particular when K_1 is large compared to K_3. Examples of double-twist geometry are nonsingular disclinations of strength $k = 2$ in cholesteric spherulites (often observed in biopolymers) that are discussed later.

Another geometry with double twist is met in the chromosome of microscopic algae, *Prorocentrum Micans* (dinoflagellate chromosomes), which have been studied by optical and electron microscopy techniques [22]. As proposed in [19] (see also [23]), the structure contains two $k = \frac{1}{2}$ disclination lines which rotate helically about the chromosome axis. The double-twist geometry has a limited size, beyond which double twist decreases and frustrations in the system become too large. The layers have a negative Gaussian

curvature. This geometry is favored over the spherulitic geometry, probably when K_1 is smaller than K_3, because the $k = \frac{1}{2}$ lines cause splay. Also, while the nucleation of the $k = 2$ geometry is easier with $K_{24} > 0$, it is the contrary to the chromosome. For a more general discussion, see review [24] on the problem of frustration.

Finally, if K_{24} is positive and very large, the cylindrical geometry can become stable versus the cholesteric phase: this is the origin of the *blue phases* (BPs). In Figure 5.4, as the distance from the Z-axis increases, the cholesteric cylindrical shells become flatter and the double twist smoothly disappears. The director far-field distribution becomes closer to the one-dimensional twist of the usual cholesteric phase; the energy gain is reduced. Thus the double twist cannot be extended over the whole three-dimensional space. A typical radius of the energy-gaining cylindrical region about the n_0-axis is the half-pitch $p/2$. (This is the reason why we discuss the double twist as a weakly twisted structure; the situation should not be confused with the fact that the blue phases usually occur for small-pitch materials). Now these cylinders of finite radius cannot tile space continuously. According to the current models of blue phases, this frustration is relieved by defect lines (of disclination type), either regularly distributed, or in disorder. Figure 5.4 illustrates how three cylinders of double twist generate a singularity in the region where they merge. A word of caution should be said about the interpretations of planar disclination lines as a source of saddle-splay. There is no K_{24} nor K_{13} contribution to the elastic energy of a straight planar disclination of the Frank type, $(n_x, n_y, n_z) = (\cos k\varphi, \sin k\varphi, 0)$, where k is integer or half-integer. Both terms vanish when the energy density is integrated over the azimuthal angle around the disclination core. A nonvanishing saddle-splay energy might come from the regions where the disclinations cross or from point defects, if such are present.

The blue phases of types BPI and BPII are modeled as regular networks of disclination lines with periodicity of order p. Indeed, the three-dimensional periodic structure of these phases is revealed in their nonzero shear moduli, their ability to grow well-faceted monocrystals and Bragg reflection in the visible part of the spectrum (which is natural since p is of the order of a few tenths of a micron). The third identified phase, BPIII, that normally occurs between the isotropic melt and BPII, is less understood. It might be a melted array of disclinations. Note that although most blue phases have been observed in thermotropic systems, double-twist geometries are relatively frequently met in textures of biological polymers, like DNA.

DNA, polypeptides (such as PBG mentioned above), and polysaccharides (such as xanthan) and many other biological and nonbiological polymers have a definite handedness due to the chiral centers. Rod-like long molecules of these materials in water solutions often crystallize into a hexagonal columnar phase so that the cross-section normal to the rods reveals a triangular lattice. Since the polymers are chiral, close hexagonal packing competes with the tendency to twist [25], [26]. Macroscopic twist can proliferate by
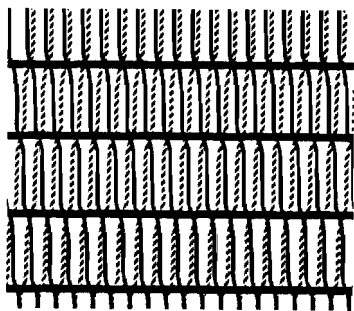
FIGURE 5.5. Coexistence of twist and close hexagonal packing in a system of chiral rods that form a twist grain boundary phase with lattices of screw dislocations; unidirectional twist perpendicular to the plane of the figure; redrawn following [27].

introducing screw dislocations into the system [27], [28], in a way akin to the twist grain boundary phases of chiral smectics [29], [30]. Two types of defect-stabilized phases that combine close packing and twist are possible. One is a polymer tilt grain boundary phase, a direct analog of the twist-grain boundary phase, and a usual cholesteric with a unidirectional twist, Figure 5.5. Another is a Moiré grain boundary phase, similar to the blue phases with double twist. In the center of a cylindrical element, there is a polymer rod; the neighboring polymers twist around it, preserving the hexagonal close packing; the cylinders are packed together thanks to the honeycomb lattice of screw dislocations [27].

For a detailed discussion of the frustrated phases, such as blue, TGB, and chiral columnar phases, see the chapters by Bock, Crooker, Kitzerow, and Pieranski.

5.4   Twisted Strips

An adequate description of defects in ordered condensed media requires introducing a special mathematical apparatus, viz. the theory of homotopy, which is a part of algebraic topology. It is precisely in the language of topology that it is possible to associate the character of the ordering of a medium and the types of defects arising in it, to find the laws of decay, merger, and crossing of defects, and to trace out their behavior during phase transitions, etc. The key point is occupied by the concept of a *topological invariant*, often also called a *topological charge*, which is inherent in every defect. The stability of the defect is guaranteed by the conservation of its topological invariant. The following simple example of twisted ribbon strips gives a flavor of the concept of a topological invariant.

5.4.1   Topological Charges Illustrated with Twisted Strips

Consider a set of closed elastic strips. Each strip is characterized by a number k that counts the number of times the ends of the strip are twisted by 2π before they are glued together to produce a ring, Figure 5.6. The ring with
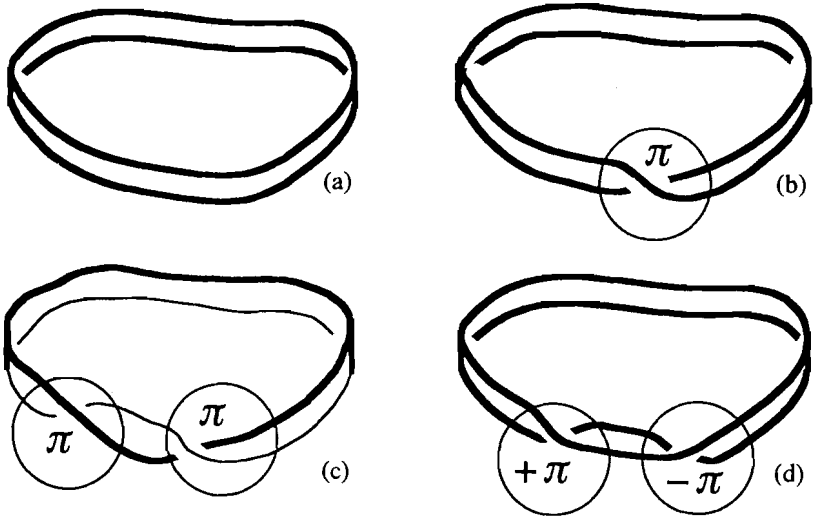
FIGURE 5.6. Topologically different rings of elastic strips: (a) nontwisted ring, $k = 0$; (b) Möbius strip, $k = \frac{1}{2}$; (c) twisted strip with two different edges, $k = 1$; and (d) twisted strip with two twists of opposite sign, $k = 0$.

$k = \frac{1}{2}$, Figure 5.6(b), is the well-known Möbius strip. The deformation energy stored in any twisted strip is larger than the pure bend energy of the $k = 0$ ring. However, to transform a twisted strip into a state $k = 0$, one needs to cut the strip. There is no continuous deformation that transforms one strip into another if the two have different k's. The energy needed to cut the ribbon, $F_{\text{cut}} \sim US/a^2$, is much higher than the stored twist energy $F_{\text{twist}} \sim k^2 KS/L$; here L is the length of the strip, S is its cross-sectional area, and $K \sim U/a$ is some elastic constant of the order of the intermolecular energy; a is the molecular scale. Transitions between the states with different k's are prohibited by high-energy barriers.

The allowed values of k are defined by the inner symmetry of the strip. For example, if the edges of the strip are different, e.g., marked by a thin line and a thick line, Figure 5.6(c), then only integer k's (2π-twists) are allowed.

The quantity k does not change under any continuous transformation and is a useful invariant to label topologically different states. Left and right twists can be distinguished by the sign of k. Obviously, one can create a pair of left and right twists without cutting the strip, Figure 5.6(d); what matters is the total sum of k's, which should be preserved. Therefore, topological charges k's obey a conservation law.

"Topological twists" considered above obey the following rules, that generalize to all types of topologically stable configurations:

(1) defect types are related to the type of ordering of the system;
(2) defects are characterized by quantized invariants (topological charges) such as k; and
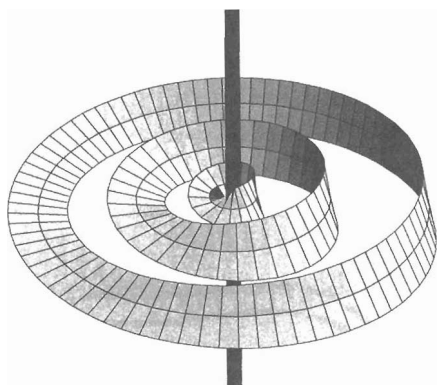
FIGURE 5.7. Disclination line with a π-twist of the director field.

(3) merger and decay of the defects are described as certain operations (e.g., additions) applied to their charges; conservation laws of topological charges control the results of merger and decay. The topological invariant k's form groups.

The topological stability of twisted strips is similar to that of topological solitons; the issue of a singular core is not involved. However, one can draw a parallel between the twisted strips and singular defects, too. Imagine a circle around a π-disclination in a uniaxial nematic liquid crystal, Figure 5.7. The set of molecules centered in this circle form a Möbius strip with $k = \frac{1}{2}$. After going once around the circle, the director $\mathbf{n}$ flips into $-\mathbf{n}$, which is possible, since the nematic bulk is centrosymmetric, $\mathbf{n} \equiv -\mathbf{n}$. The number k would remain equal to $\frac{1}{2}$ whether the radius of the circle is taken larger or smaller, Figure 5.7. Thus the overall director configuration can be characterized by $k = \frac{1}{2}$ (k is often called the "strength" of the disclination). At the disclination core, one faces the singularity: when the circle shrinks into a point, there is an infinity of director orientations at this point. This rule of exact transformation $\mathbf{n} \rightarrow -\mathbf{n}$ does not change if the nematic is replaced by a cholesteric.

5.4.2   DNA Loops

Twisted strips with different k's are of relevance to the problem of configuration and replication of double-stranded DNA molecules. Two strands are arranged in a helicoid fashion in which a 2π-twist occurs per every 10.5 base pairs. In many organisms ranging from viruses and prokaryotes to some eukaryotes, DNA molecules form closed loops. Topologically, these loops remind us of a twisted strip with *two distinctive* edges, carrying a special integer *Lk*, referred to as *the linking number* of the two edges. It is an algebraic (i.e., accounting for the direction) number that shows how many times one (line) edge crosses a surface spanning the other (line) edge [31]. *Lk*

is peserved in any conformational change of the DNA molecule that does not break the strands. If Lk is close to $Lk_0 = l/p$ (l is the total DNA length, and $p \approx 3.4$ is the helix pitch), the DNA ring is elastically relaxed and can lie flat on a planar surface without contortion. Often $Lk \neq Lk_0$: the ends of the relaxed linear DNA duplex might be additionally twisted (or untwisted) by some number of rotations $\pm 2\pi$ before forming the ring. There are two ways of dealing with the induced strain. First, the number of base pairs per pitch can be changed; the ring remains *planar* and the linking number is equal to the number of turns of one strand around another. In that case, $Lk = k$, the *topological* twist defined above. Second, the duplex axis can twist upon itself, leaving the number of pairs per pitch unaffected. Such a *supertwisted* DNA is no longer planar and coils in three dimensions, like a buckled twisted ribbon. Whatever the case, while k and Lk stay unaffected, and are still equal integral numbers of a *topological* nature, the global *geometry* (and consequently the energy of the "twisted" ribbon and the way it relaxes) depends on the elasticity properties of the molecule and is better described by two *geometrical* parameters: the (so-called) *twist Tw* and the *writhe Wr*. The twist can be written as

$$Tw = \frac{1}{2\pi} \oint \Omega(s)\, ds, \tag{5.14}$$

where $\Omega(s)$ is the rate of wrapping of either strand about the duplex axis (the angle of rotation of the base pairs the per unit length of the strand). This quantity can be defined equally for an open strip; Tw can take any value and we can refer to it as the *geometrical* twist. However, if the duplex axis is planar, one gets $Lk = Tw = k$. The writhe Wr of a curve C is a much more subtle quantity. Introduced by Fuller [32], it is the number of averaged self-crossings (with sign) of the planar orthogonal projections of C (closed or not); in the DNA context it describes the buckling of the duplex axis, so to speak. Like Tw, Wr can take any value. We have the important relation

$$Lk = Tw + Wr \tag{5.15}$$

with Lk (for two oriented curves C and C') and Wr (for an oriented curve C) given by double integrals:

$$Lk = \frac{1}{4\pi} \oiint_{C,C'} \frac{\mathbf{r}(s) - \mathbf{r}(s')}{|\mathbf{r}(s) - \mathbf{r}(s')|^3} . [d\mathbf{s} \times d\mathbf{s}'];$$

$$Wr = \frac{1}{4\pi} \oiint_{C,C} \frac{\mathbf{r}(s) - \mathbf{r}(s^*)}{|\mathbf{r}(s) - \mathbf{r}(s^*)|^3} . [d\mathbf{s} \times d\mathbf{s}^*]. \tag{5.16}$$

Here C is the duplex axis, say, and C' is any one of the strands. Wr vanishes when C is planar. Applications of these mathematical concepts to the elasticity of DNA can be found in [33].

To separate the DNA strands during replication, one needs to change the number Lk. It can be done directly by topoisomerases that cut one or both

strands. In other cases, the replication occurs through local binding of the DNA molecule to proteins that creates zones of negative and positive supertwisting; for more details, see [34].

5.5   Line Defects—Disclinations and Dislocations

Generally, the order parameter of an ordered medium is a function of coordinates, $\psi(\mathbf{r})$. Distortions of $\psi(\mathbf{r})$ can be of two types: those containing singularities and those without singularities. At singularities, ψ is not defined. For a three-dimensional (3D) medium, the singular regions might be zero-dimensional (points), one-dimensional (lines), or two-dimensional (walls). These are the *defects*. Whenever a nonhomogeneous state cannot be eliminated by continuous variations of the order parameter (i.e., one cannot arrive at the homogeneous state), it is called *topologically stable*, or simply a *topological defect*. If the inhomogeneous state does not contain singularities, but nevertheless is not deformable continuously into a homogeneous state, one says that the system contains a *topological configuration* (or *soliton*). The twisted wedge geometry considered in Section 5.2.1 is topologically trivial and equivalent to a uniform nematic. In contrast, point defects in droplets or defects involved in the formation of blue phases and twist grain boundary phases are topologically stable.

The topological classification of line defects in ordered media is based on the concepts of the order parameter (OP) space $\mathfrak{R}$ and homotopy groups of the OP space [35]–[38]. Line defects are described by the so-called first (or fundamental) homotopy group $\pi_1(\mathfrak{R})$. Topological invariants labeling different defect lines are elements (or *classes* of elements) of $\pi_1(\mathfrak{R})$. Point defects are described by the second homotopy group $\pi_2(\mathfrak{R})$. This group is trivial for cholesterics, so that there is no topological point defect. Below we consider only line defects. We start with a uniaxial nematic, for which the predictions of topological classification are rather simple (the results can be applied to a weakly deformed cholesteric, such as a 90° twisted nematic cell).

5.5.1   Disclinations in the Uniaxial Nematic

The OP space $\mathfrak{R}$ is the manifold of all possible values of the OP that do not alter the thermodynamical potentials of the system. The energy of condensation F_{cond} takes a minimum value on $\mathfrak{R}$. For a uniaxial nematic, the OP space is a sphere of unit radius: any point on the sphere corresponds to a different orientation of the director $\mathbf{n}$. Furthermore, since $\mathbf{n} \equiv -\mathbf{n}$, any two diametrically opposite points on the sphere describe not just energetically equivalent states, but rather indistinguishable states. The unit sphere with identified antipodal points is denoted S^2/Z_2; it is the OP space of a uniaxial nematic.

Suppose that the nematic is deformed so that the director becomes a
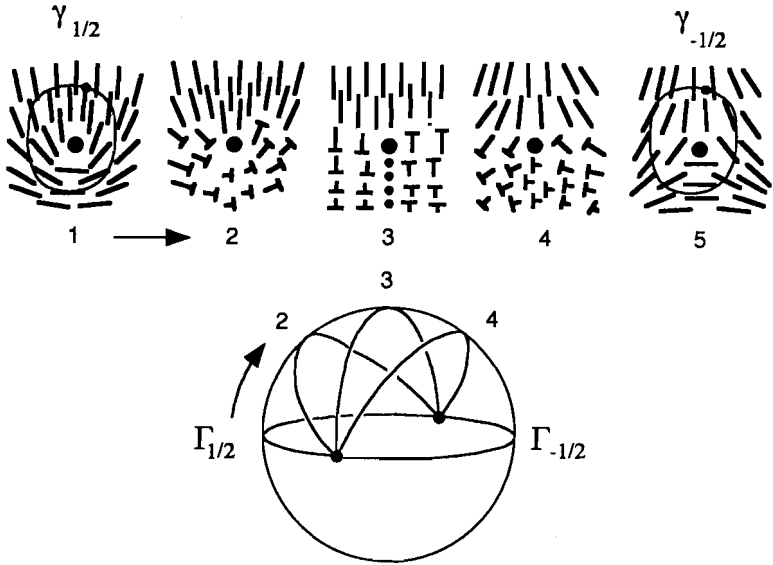
FIGURE 5.8. Continuous transformation of a disclination $k = \frac{1}{2}$ into a disclination $k = -\frac{1}{2}$ in real space (director configurations above) and the corresponding transformation of contours in the OP space S^2/Z_2.

function of the coordinates. The function $n(r)$ maps the points r occupied by a sample in real space into the OP space. In the classification of line defects, the mappings of interest are those of oriented contours encircling defects in real space. For example, in Figure 5.8, the contour $\gamma_{1/2}$ is mapped into the contour $\Gamma_{1/2}$ in the OP space.

The mapping $n(r)$ of a closed contour in real space produces in the OP space S^2/Z_2 a contour which belongs necessarily to one of the following classes: either (a) a closed loop, or (b) a contour that connects two diametrically opposite points; this contour is closed because the two end points are identical. The contours of type (a) can shrink into a point; they correspond to disclinations of integer strength k which are topologically unstable and can be smoothly transformed into a uniform state through the well-known process [39], [40] that R.B. Meyer called "escape in the third dimension" [40]. The contours of type (b) are not contractible to a point under any continuous deformations, since the ends of the contours have to remain fixed at diametrically opposite points. These contours correspond to disclinations of half-integer strength k.

It is easy to see that all the contours corresponding to half-integer k's can be smoothly transformed one into another, Figure 5.8. The classes (a) and (b) of contours form a group Z_2 of two elements, say, 0 and $\frac{1}{2}$. The group operation laws are simply $\frac{1}{2} + 0 = \frac{1}{2}$ and $\frac{1}{2} + \frac{1}{2} = 0$. The group of closed con-

tours is called a fundamental group of the OP space and denoted $\pi_1(\mathfrak{R})$. For a uniaxial nematic

$$\pi_1(S^2/Z_2) = \dot{Z}_2, \qquad (5.17)$$

which means that there is only one type of topologically stable line disclination.

On one hand, each element of the homotopy group corresponds to a class of topologically stable defects; all defects belonging to the same class are equivalent to one another under continuous deformations. On the other hand, the elements of homotopy groups are topological invariants, or topological charges of the defects. The defect-free state corresponds to a unit element of the homotopy group and to a zero topological charge. There is no possibility of transforming a configuration from one class into a configuration from another class: transformations $\frac{1}{2} \leftrightarrow 0$ are prohibited by (infinitely) high energy barriers. In contrast, transformations $\frac{1}{2} + \frac{1}{2} \leftrightarrow 0$ are topologically possible; whether they happen or not depends on energies that are of the order of disclination energy or smaller.

Let us now consider how the chiral asymmetry changes the classification.

5.5.2   Disclinations in the Cholesteric Phase

Additional interactions, such as dielectric coupling to the electric field, surface anchoring, biaxial or chiral interactions, with energy $F_{int} < F_{cond}$, change the OP space from $\mathfrak{R}$ to some $\bar{\mathfrak{R}}$ at which the sum of energies $F_{cond} + F_{int}$ is minimum. $\bar{\mathfrak{R}}$ is a submanifold of $\mathfrak{R}$ [37]. Chiral asymmetry of the molecules leads to the transition from a nematic state with $\mathfrak{R} = S^2/Z_2$ which carries all the possible rotations of a unique director, to a cholesteric state with $\bar{\mathfrak{R}}$ which carries all the possible rotations of a set of three mutually perpendicular directors. To comply with the terminology of Friedel and Kléman [41], we will denote these directors λ (which shows the local direction defined by the molecule), χ (along the helical axis), and $\tau = \lambda \times \chi$. The OP space is the group $G = SO(3)$ of rotations of the trihedron λ, χ, τ, factored by the four-element point group D_2 of π rotations about the directions λ, χ, and τ:

$$\bar{\mathfrak{R}} = SO(3)/D_2. \qquad (5.18)$$

The same result can be obtained for biaxial nematics [42]: from a topological point of view, the classifications of defects in cholesterics and biaxial nematics are identical. Calculation of the fundamental group for $\bar{\mathfrak{R}} = SO(3)/D_2$ requires knowledge beyond the scope of this chapter. We simply present the result (for details, see [2], [37], [42]):

$$\pi_1(\bar{\mathfrak{R}}) = Q. \qquad (5.19)$$

Q is the group of quaternion units which consists of eight elements $\{I, J, i, -i, j, -j, t, -t\}$ that obey the multiplication rules:
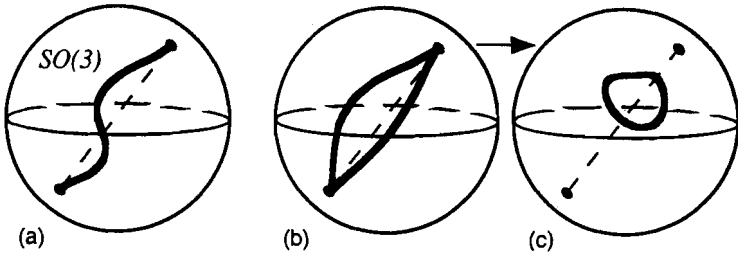
FIGURE 5.9. Closed contours (a) Γ_1 and (b), (c) Γ_2 corresponding to $|k| = 1$ and $|k| = 2$ disclinations in the OP space of the cholesteric. Both contours connect diametrically opposite and equivalent points at the surface of $SO(3)$. Γ_1 cannot continuously shrink into a point. Γ_2 runs between the two antipodal points twice (b) and can smoothly leave these points and shrink into a point (c).

$$ij = -ji = t, \qquad jt = -tj = i, \qquad ti = -it = j,$$
$$JJ = I, \qquad ii = jj = tt = J, \qquad ijt = J. \qquad (5.20)$$

The multiplication rules dictate how the disclinations merge, split, and transform. Note that the group operation is noncommutative, i.e., Q is a non-Abelian group. Because of this, each disclination in a cholesteric is characterized not by an element of the fundamental group but by a *class* of conjugate elements of Q. There are five conjugacy classes: $C_0 = \{I\}$, $\bar{C}_0 = \{J\}$, $C_\lambda = \{i, -i\}$, $C_\tau = \{j, -j\}$, and $C_\chi = \{t, -t\}$. Correspondingly, the topological charge acquires the values 1; -1; $(i, -i)$; $(j, -j)$; $(t, -t)$.

Classes C_λ, C_τ, and C_χ correspond to π rotations of directors when one goes once around the disclination's core; for example, C_λ relates to rotations of χ and τ (λ remains nonsingular). Class $\bar{C}_0$ corresponds to 2π rotations; unlike their nematic counterparts, these lines are topologically stable. Class C_0 describes topologically unstable 4π disclinations.

The striking difference between 2π (stable) and 4π (unstable) lines is illustrated in Figure 5.9. The difference between 2π and π (both stable) lines can be illustrated by the following example [43] with χ lines (no singularity in the χ field). Suppose the χ line is perpendicular to equidistant cholesteric layers. The OP space for the nematic director is then S^1/Z_2, which implies an infinite number of topologically distinct χ lines with integer and half-integer k. When one approaches the core region of the line, the elastic energy $\sim K(\nabla \mathbf{n})^2$ increases, until at distances $\sim p$ it becomes comparable to the energy difference $\sim K/p^2$ between the cholesteric and nematic states. At scales smaller than $\sim p$, the OP space of the nematic director reverts to S^2/Z_2. Therefore, the 2π lines with integer k should have a thick core of typical diameter $\sim p$ that is nonsingular from the nematic point of view: the director is uniform (escaped in third dimension) inside the cylinder of diameter $\sim p$. In contrast, π lines with half-integer k are singular both for the uniaxial

TABLE 5.1. Multiplication rules of five classes of elements of the group Q that control the merger and splitting of disclinations in a cholesteric phase.

	C_0	$\bar{C}_0$	C_λ	C_τ	C_χ
C_0	C_0	$\bar{C}_0$	C_λ	C_τ	C_χ
$\bar{C}_0$	$\bar{C}_0$	C_0	C_λ	C_τ	C_χ
C_λ	C_λ	C_λ	C_0 or $\bar{C}_0$	C_χ	C_τ
C_τ	C_τ	C_τ	C_χ	C_0 or $\bar{C}_0$	C_λ
C_χ	C_χ	C_χ	C_τ	C_λ	C_0 or $\bar{C}_0$

nematic and cholesteric OPs. Interestingly, the π lines with half-integer k can be further shown to be nonsingular if one allows for biaxiality of the nematic phase and compares the gradient energies at the core to the energy difference between the uniaxial and biaxial states [44]. As a result, in typical thermo-tropic materials, the core of π lines can be about an order of magnitude wider than the molecular length [44].

The multiplication rules (5.20) are specific of the classes of elements, rather than the elements themselves. The results are given in Table 5.1, that can be used to predict the result of merger or splitting of disclinations.

If two disclinations from two different classes merge, the resulting dis-clination belongs to the class of the product of the first two. The merger of disclinations of the same class from the set C_λ, C_τ, C_χ is ambiguous: the result is either a trivial configuration (class C_0) or a disclination from class $\bar{C}_0$, depending on the path of merger with respect to other defect lines in the system [37].

The energy of disclination strongly depends on how the trihedron λ, χ, τ is distorted. In a uniaxial cholesteric, the three have different physical meaning and different distortion energy. Only λ is a real director while τ the χ are "immaterial" directors; singularities C_τ and C_χ would be generally more costly than C_λ.

The difference is seen when the disclinations of half-integer strength $k = n + \frac{1}{2}$ (n is an integer) are compared. The so-called λ disclinations in which the director λ is not singular are apparently less energetically costly than τ disclinations in which λ is singular. The core of λ disclinations is of radius p ("thick" lines), Figure 5.10(a), (b), (d), while the core of τ dis-clinations ("thin" lines) is of molecular size (or somehow larger, as discussed above), Figure 5.10(c). The line tensions thus differ by an amount $\sim K \ln(p/a)$, where a is of the order of 1–10 molecular sizes. If the cholesteric is unwound into a nematic phase, $p \to \infty$, then λ disclinations vanish. A λ^- (where the superscript "$-$" indicates that the line is of negative strength $k = -\frac{1}{2}$) can be annihilated by a collapse with a λ^+, Figure 5.10(b). Figure 5.10(c) pictures a τ^+, i.e., a wedge line of strength $k = \frac{1}{2}$, singular for the χ and λ fields but continuous for the τ field. χ lines will be discussed in the next subsection, since they can be treated as dislocations in the system of cholesteric layers.
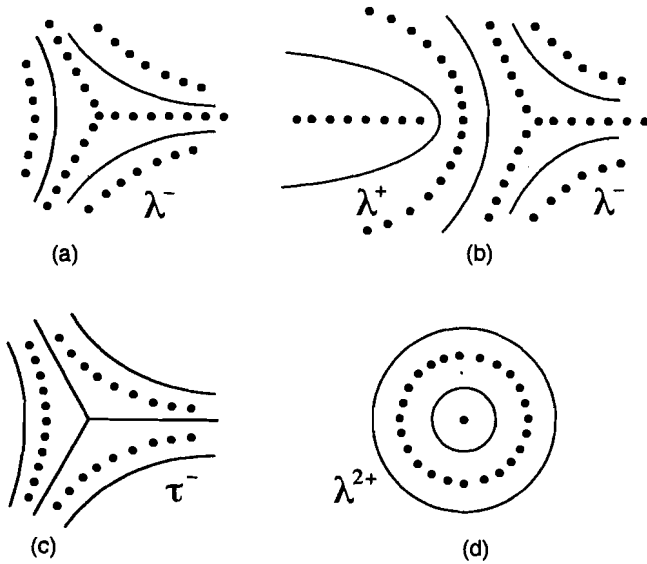
FIGURE 5.10. Disclinations λ and τ in a cholesteric.

The disclinations of integer strength belong to two different classes: those of odd strength $k = 2n + 1$ and those of even strength $k = 2n$. As already mentioned, the disclinations $k = 2n + 1$ cannot be eliminated; the escape of the director into the third dimension is restricted by a region of size $\sim p$. As is clear from Figure 5.10(d), the λ line with $k = 1$ cannot be made continuous for the two fields τ and χ simultaneously. If, say, the τ field is made continuous, then the χ field remains singular. In contrast, $k = 2n$ lines do escape in the third dimension, Figure 5.9. The distribution of λ, τ, and χ disclinations of different strength among the five classes of the quaternion group Q is summarized in Table 5.2.

The topological classification prohibits transformations of disclinations from one class to another. For example, $\tau(n + \frac{1}{2})$, $\lambda(n + \frac{1}{2})$, and $\chi(n + \frac{1}{2})$ cannot be continuously transformed one into another, despite the apparent similarity in the value of the "strength." On the other hand, different lines can be transformed by splitting. For example, according to Table 5.1 and

TABLE 5.2.

C_0	$\bar{C}_0$	C_λ	C_τ	C_χ
$b = -2np$	$b = -(2n+1)p$			$b = -(n+\frac{1}{2})p$
$\lambda(2n)$	$\lambda(2n+1)$	$\lambda(n+\frac{1}{2})$		
$\tau(2n)$	$\tau(2n+1)$		$\tau(n+\frac{1}{2})$	
$\chi(2n)$	$\chi(2n+1)$			$\chi(n+\frac{1}{2})$

(5.20), a C_τ line can split into a pair of C_λ and C_χ lines, if it saves elastic energy. An example of such a splitting (of χ lines into $\lambda\tau$ pairs) will be discussed in the next Section 5.5.3. There is no violation of the law of conservation for the strength k in all these processes since k is not a conserved topological invariant, but just a useful label to distinguish different configurations.

One should bear in mind that the topological classification of defects in cholesteric and other layered media such as smectics and ordinary crystals is limited by the condition of the layers equidistance. As a result, some transformations between defects that belong to the same class require very high energy barriers comparable to the energy barriers between different classes. Transformation $\lambda^+ \leftrightarrow \lambda^-$ within the class C_λ represents such an example.

Disclinations λ and τ are often observed in fingerprint textures. Since the line tension of the λ lines (with a nonsingular core of size $\sim p$) is smaller than the line tension of the singular τ lines by an amount $\sim K\ln(p/a)$, one would expect that λ defects are more frequent. However, this analysis might be altered if the cholesteric phase is biaxial: then all three directors might have the same energy weight. Livolant [45] has extensively studied disclinations in the cholesteric textures of three helical biological polymers: DNA, PBG, and xanthan: the λ lines were quite frequent, while isolated τ lines have never been observed. On the other hand, the τ disclinations often appear in pairs with λ disclinations to replace χ disclinations.

5.5.3   Dislocations

The symmetry of rotations $n\pi$ around the χ-axis in cholesterics is equivalent to the symmetry of translations $n(p/2)\chi$. Therefore, the χ disclinations can be equivalently treated as dislocations [10], [46], with the Burgers vector

$$b = -kp. \tag{5.21}$$

The values of the Burgers vector are included in Table 5.2. Figure 5.11(a) pictures a χ^+ wedge disclination (χ is continuous). It can be constructed by a Volterra process performed along the line, by opening the cut surface by an angle π: each cholesteric layer yields a two-dimensional $k = \frac{1}{2}$ configuration that rotates helically along the line with a pitch p.

The equivalence just demonstrated for screw dislocations versus wedge χ disclinations can be extended to edge dislocations (Figure 5.12) versus twist χ disclinations and even further, to mixed dislocations and disclinations, for the simple reason that the two corresponding Volterra processes are the same.

An important property of χ dislocations is their ability to split into combinations of λ and τ disclinations. Of course, these transformations must obey the multiplication rules (5.23). For example, a χ line from the class C_χ can split into a pair of λ and τ lines (classes C_λ and C_τ, respectively). An example is shown in Figure 5.11(b), (c): the core splits into a λ^- and τ^+
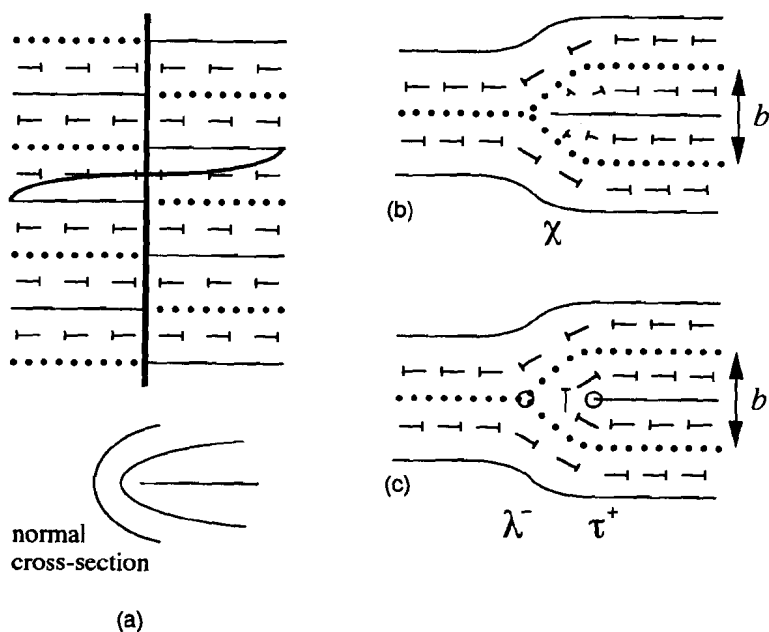
FIGURE 5.11. Equivalence in the presentation of χ lines: (a) wedge χ^+ disclination = screw dislocation; (b) χ-twist disclination = edge dislocation; and (c) splitting of the core of a dislocation into a pair of disclinations.

separated by a distance $p/4$; the Burgers vector is $b = p/2$, i.e., twice the distance of pairing. Figure 5.12 shows a split dislocation with $b = p$.

Splitting of a dislocation into two disclinations of strength $|k| = \frac{1}{2}$, i.e., of rotation $\pm\pi$, relates to the fact that the product of two opposite π rotations along two parallel axes Ω and $-\Omega$ ($|\Omega| = 1$) at a distance $\mathbf{d}$ is a translation

$$\mathbf{b} = 2\Omega \times \mathbf{d}. \tag{5.22}$$

Therefore, two π disclinations of opposite signs $L(\Omega)$ and $L'(-\Omega)$ are altogether equivalent to a dislocation $L(\mathbf{b})$; the "core" of the dislocation extends over L and L'.

Splitting of χ disclination lines has been observed in the so-called "Cano" wedges: one of the disclinations is always a λ, i.e., it does not carry any material singularity. The first dislocations near the center of the wedge have a small Burgers vector ($b = p/2$), while b increases for dislocations far from the center.

When the cholesteric layers are tilted with respect to the bounding plate, the disclinations might occur to match the twisted structure in the bulk with an (usually unidirectional or conical) orientational field of anchoring forces [47]–[49]. Here again, the χ dislocations split into λ and τ pairs. The λ lines
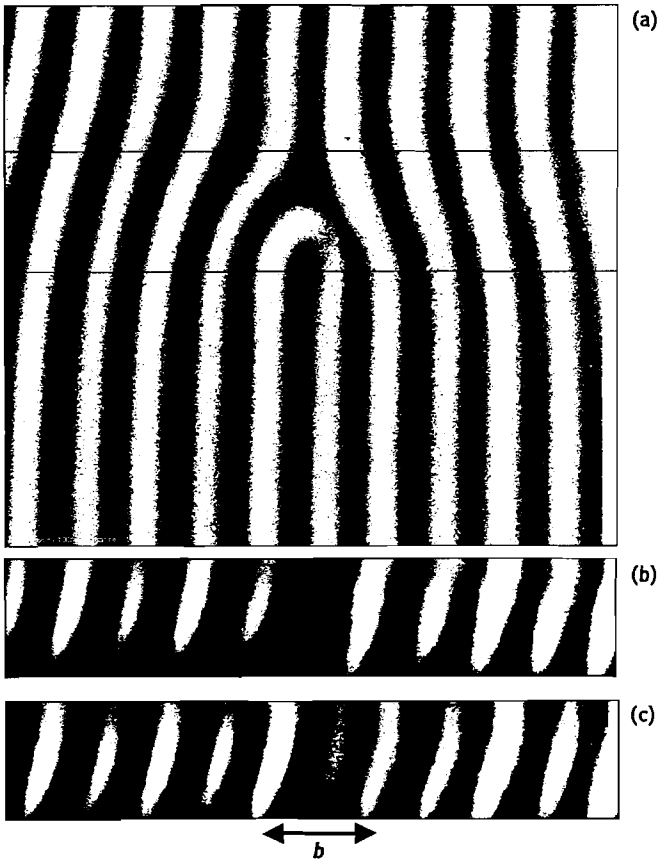
FIGURE 5.12. Confocal-microscope image of a dislocation $b = p$ in the "fingerprint" cholesteric texture. The confocal microscope technique allows one to obtain the image of the director pattern not only (a) in the plane of the sample but (b), (c) in the vertical cross-section as well (photo D. Voloschenko).

are in the bulk while the τ lines are at the surface (which reduces their energy).

5.5.4   Entanglement of Disclinations

One of the most spectacular consequences of noncommutativity of the group Q is the possibility of a topological entanglement of the disclinations. Originally, the problem was considered by Toulouse for biaxial nematics [42], but it applies to any medium with a non-Abelian fundamental group [50]–[52].

Figure 5.13(a) shows two entangled disclinations. The question is whether they can be transformed by continuous variations of the directors into an
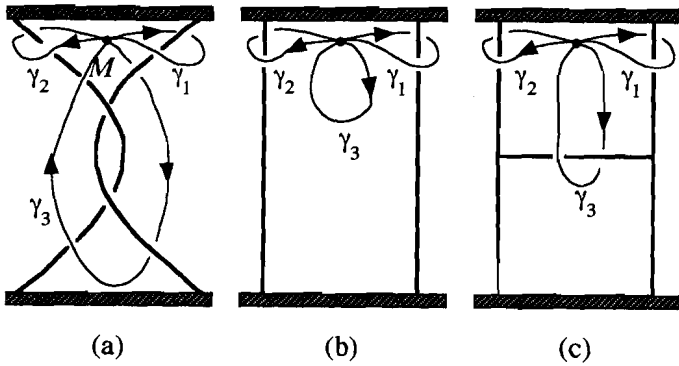
FIGURE 5.13. (a) Entanglement of disclinations in a medium with a trihedron of vectors as the order parameter; (b) topologically trivial; and (c) nontrivial.
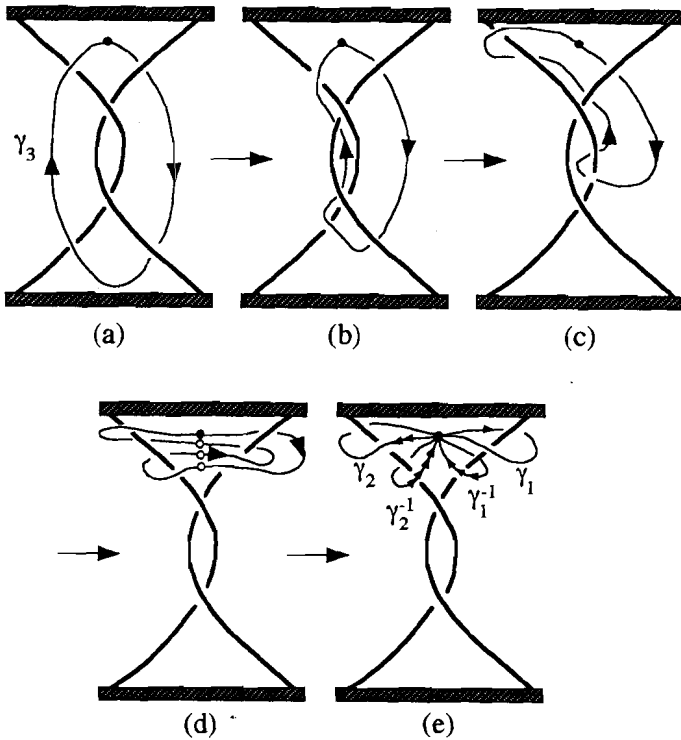
FIGURE 5.14. Continuous deformations of the contour γ_3 from Figure 5.13 into the product contour $\gamma_1\gamma_2\gamma_1^{-1}\gamma_2^{-1}$ demonstrating that the image Γ_3 of γ_3 in OP space is homotopic to the product $\Gamma_1\Gamma_2\Gamma_1^{-1}\Gamma_2^{-1}$. At step (d), one pinches together four points marked by circles.

unlinked configuration, Figure 5.13(b), if we require that the ends of the disclinations remain fixed.

To find the answer let us draw three contours γ_1, γ_2, and γ_3 from a point M of real space: γ_1 and γ_2 encircle the defect lines and γ_3 encircles the entangled region, Figure 5.13. Their images in OP space will be some contours Γ_1, Γ_2, and Γ_3. Evidently the defects can be unlinked only when Γ_3 is homotopic to zero. If this is not so, then separation of the disclinations will leave a topologically nontrivial trace in space, a third disclination, Figure 5.13(c). The result depends on the nature of the linked disclinations. One can show, Figure 5.14, that the contour Γ_3 is homotopic to the product $\Gamma_1\Gamma_2\Gamma_1^{-1}\Gamma_2^{-1}$; an element of this form is called a commutator in the fundamental homotopy group. For Abelian groups the commutator is the identity element, since $\Gamma_1\Gamma_2 = \Gamma_2\Gamma_1$. This is not true for non-Abelian groups; in particular, for the group Q the contour Γ_3 can belong either to the class C_0 ($\Gamma_1\Gamma_2\Gamma_1^{-1}\Gamma_2^{-1} = 1$) or to the class $\bar{C}_0$ ($\Gamma_1\Gamma_2\Gamma_1^{-1}\Gamma_2^{-1} = -1$). The latter situation occurs when the two entangled disclinations belong to different classes from the set C_λ, C_τ, C_χ. Therefore, after pulling two different disclinations $|k| = \frac{1}{2}$ across one another, they prove to be connected by a disclination $|k| = 1$ belonging to $\bar{C}_0$.

5.6   Effects of Confinement

Topological defects are often needed to equilibrate an ordered system. There are two different possibilities here. First, the defects can occur to relieve intrinsic ("bulk") frustrations (for instance, between the twist and layered structures in TGB phases). Second, the defects can occur simply because the system is bounded or because there are foreign inclusions, such as colloidal particles or droplets in a liquid–crystalline host.

Surface interactions (the phenomenon known as anchoring) change the OP space. One can imagine, for example, a cholesteric bounded by a flat wall that imposes strictly normal director orientation. No uniform cholesteric structure of type (5.1) can satisfy this boundary condition; resulting distortions might involve defects. However, this is not the case we have in mind. What we have in mind is that topological defects must appear in the equilibrium state when the bounding surface has a nonzero Euler characteristic. Similar analysis can be performed for particles of different topology dispersed in the liquid crystal matrix. The condition for this topological consideration to be valid is that the characteristic size of the liquid–crystal system or the dispersed droplet is larger than the anchoring extrapolation length, as will be discussed later.

Suppose a two-dimensional vector field $\mathbf{n}$ is defined on a closed surface with Euler characteristic E. This field might contain point defects whose topological charges are defined as

$$N^{(2)} \equiv k = \frac{1}{2\pi} \oint \left(n^1 \frac{dn^2}{dl} - n^2 \frac{dn^1}{dl} \right) dl = 0, \pm 1, \pm 2, \ldots, \qquad (5.23)$$

where l is a natural parameter defined along the loop enclosing the defect point on the surface. Number k shows how many times $\mathbf{n}$ rotates by an angle 2π when one moves around the defect once.

The *Poincaré theorem* states that the sum of all charges k of the field $\mathbf{n}$, defined at a closed surface, is equal to the Euler characteristic of the surface

$$\sum_j k_j = E. \qquad (5.24)$$

For a sphere, $E = 2$; thus the two point defects at the poles of the nematic droplets in Figure 5.3 illustrate the Poincaré theorem; it does not matter if the interior structure is twisted or not.

Suppose now that the vector field is three-dimensional. There might be point defects in this field as well. A topological characteristic can be introduced as a number N which counts how many times one meets all possible spatial orientations of the vector field while moving around a closed surface surrounding the point defect. Analytically [53]:

$$N = \frac{1}{4\pi} \oiint \begin{vmatrix} n^1 & n^2 & n^3 \\ \dfrac{\partial n^1}{\partial u} & \dfrac{\partial n^2}{\partial u} & \dfrac{\partial n^3}{\partial u} \\ \dfrac{\partial n^1}{\partial v} & \dfrac{\partial n^2}{\partial v} & \dfrac{\partial n^3}{\partial v} \end{vmatrix} du\, dv = \frac{1}{4\pi} \oiint \mathbf{n} \left[\frac{\partial \mathbf{n}}{\partial u} \times \frac{\partial \mathbf{n}}{\partial v} \right] du\, dv, \qquad (5.25)$$

where the coordinates u and v are specified at the surface enclosing the defect. If the vector field is parametrized as $\mathbf{n}(u, v) = \{\sin\theta\cos\varphi; \sin\theta\sin\varphi; \cos\theta\}$, where both polar θ and azimuthal φ angles are functions of u and v, then

$$N = \frac{1}{4\pi} \oiint \left(\frac{\partial\theta}{\partial u} \frac{\partial\varphi}{\partial v} - \frac{\partial\theta}{\partial v} \frac{\partial\varphi}{\partial u} \right) \sin\theta\, du\, dv. \qquad (5.26)$$

For example, for a radial hedgehog $\mathbf{n} = \mathbf{r}$ in spherical coordinates

$$N = \frac{1}{4\pi} \oiint \sin u\, du\, dv = 1. \qquad (5.27)$$

The Gauss theorem states that if the three-dimensional vector field is normal to the closed surface of Euler characteristic E, then the sum of all point defects inside the bounded volume is

$$\sum_i N_i = E/2, \qquad (5.28)$$

i.e., 1 in the case of a sphere.

Both the Poincaré and Gauss theorems can be applied to structures in cholesteric droplets provided that the surface anchoring is sufficiently strong.
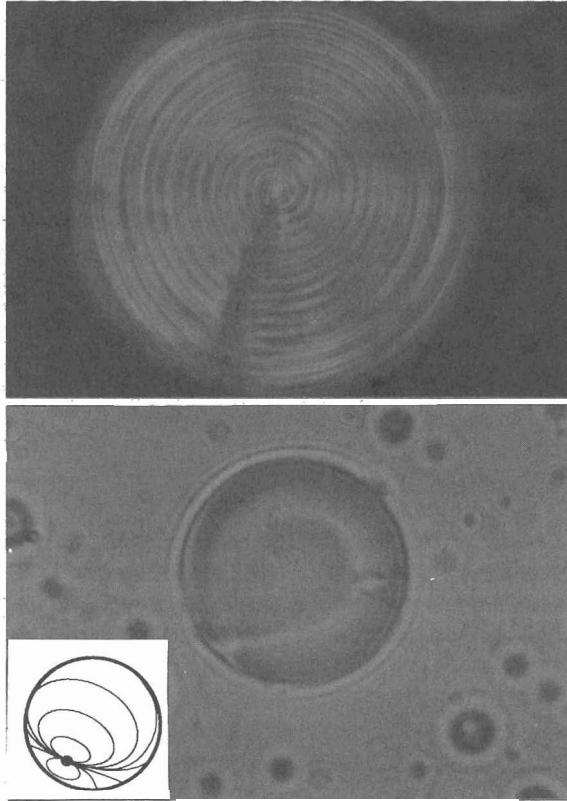
FIGURE 5.15. Cholesteric textures in spherical droplets with tangential director anchoring at the boundary. Top: A monopole configuration with a point defect $N = 1$ in the field χ of normals to the cholesteric layers and an attached nonsingular line $k = 2$, stable when $R/p \gg 1$ (microphotograph in crossed polarizers). Bottom: A boojum configuration with an isolated $k = 2$ surface point defect at $R/p \sim 1$ (no crossed polarizers). The insert shows the director field at the surface of the droplet.

That is definitely the case when the radius R of the droplet is much larger than the anchoring length K/W, where W is the anchoring coefficient (work per unit area needed to deviate the director from the anchoring direction by an angle, say, 1 rad). The reason is that the typical value of the anchoring energy (resp. the bulk elastic energy) is WR^2 (resp. KR): the surface energy overweighs the bulk elastic energy for large R. If $R \gg p$, cholesteric droplets display a monopole-type structure first observed by Robinson and explained by Frank and Price, see [54] and Figures 5.15 and 5.16. The cholesteric layers form a concentric system of spheres. The field χ of normals to the layers form a radial point-defect hedgehog with $N = 1$ in the center, as dictated by (5.28). This point defect cannot be isolated, however: according to (5.24),
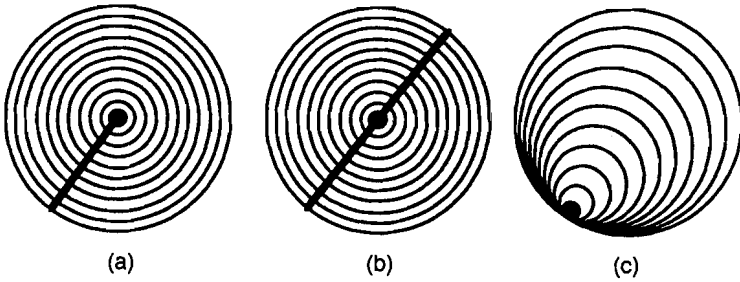
FIGURE 5.16. Configuration of layers in monopole structures with (a) one $k = 2$ or (b) two $k = 1$ disclinations; (c) boojum obtains from the monopole when the line defect shrinks into a point at the boundary.

each cholesteric layer must contain a point defect in the orthogonal fields λ and τ. These point defects form a radial line. There might be one disclination of class C_0 with $k = 2$ or two disclinations of class $\bar{C}_0$ with $k = 1$ [55]–[59]. The overall structure is reminiscent of the Dirac monopole [60], an elementary magnetic charge that carries a point defect of the magnetic field, $\mathbf{B} \| \mathbf{r}$, with an attached line singularity in the vector-potential $\mathbf{A}$. The vector-potential $\mathbf{A}$ is normal to $\mathbf{B}$ and is thus specified on the concentric spheres around the point, which again brings (5.24) into action and leads to the line singularity in $\mathbf{A}$.

The example above shows that the isolated point defects are not likely to occur in the bulk of cholesteric phase when $L/p \gg 1$. This is indeed a general statement, valid for any ordered medium, such as superfluid 3He-A, smectic C, or biaxial nematic with a trihedron of vectors as the order parameter: the second homotopy group for the OP space of these media is trivial. However, point defects *at the boundary* of the cholesteric volumes and all the media listed above are formally allowed by the homotopy theory.

The point defect at a surface of an ordered medium can represent either the end of a line that is topologically stable in the bulk or a true surface point defect with no bulk singularity attached [61]. In cholesteric liquid crystals, all points with $|k| = \frac{1}{2}; 1$ are the ends of bulk disclinations. Only when $|k| = 2$ (4π rotations of the director field), the point defect might be an isolated surface singularity. However, even in this case one should take care of the requirement of the layers equidistance. For example, the classical boojum configuration cannot be observed in a cholesteric vessel when $L/p \gg 1$.

The boojum has been introduced by Mermin [62] for superfluid 3He-A as a way of reducing the energy of the monopole. In the 3He-A spherical volume, the energy of a monopole decreases when the line shrinks into a point at the surface; this point is the boojum. However, in the cholesteric phase, such a transformation violates the equidistance between the layers. As a result, the monopole structure remains stable, at least when $R/p \gg 1$. Only when $R/p \sim 1$, can the isolated point defect with 4π rotations of the director field

be observed. Figure 5.15 shows how the cholesteric monopole is replaced by a boojum when the pitch increases [6], [55].

Cholesteric droplets have been extensively studied during the last decade, especially after Crooker and Yang suggested to use polymer-dispersed cholesteric liquid crystals for reflective color displays [63]. Lavrentovich and Nastishin [64], [65] reported on an intriguing phenomenon: liquid crystal droplets dispersed in an isotropic matrix (glycerin with lecithin) *divided* into smaller ones when one decreases the temperature of the sample, and passes from the cholesteric to the smectic A phase through the TGB phase. The reader is referred to the recent reviews [66]–[68], and to the contribution of Crawford, Svenšek, and Zumer in this book for more details about dispersed liquid crystals.

Much less is known about the inverted systems, in which the liquid crystal serves as a host to foreign particles, say, spherical silica particles or water droplets. The topological consideration above can be applied to these systems as well, as soon as the dispersed particles are large enough for the surface anchoring to set a well-defined director orientation at the particle surface. Since each spherical particle is a seed of a nonzero Euler characteristic $(E = 2)$, the topological defects are intrinsic to these systems and define many important physical features, such as stability against coagulations observed for isotropic droplets in the nematic host [69].

5.7   Nonsingular Configurations and Solitons

The concept of OP space helps us to analyze complicated configurations of the cholesteric order parameter even when these configurations are topologically trivial, i.e., equivalent to an undistorted cholesteric or nematic.

Suppose the cholesteric is confined between two homeotropic plates separated by a distance $L \sim p$. The magnetic field acts along the normal $\mathbf{h}$ to the plates. If the field is sufficiently strong, or the sample is sufficiently thin, the cholesteric is in the homeotropic nematic state with the director $\mathbf{n} = \pm\mathbf{h}$; the OP space is reduced to a single point. When the field decreases, the balance of diamagnetic, elastic, and surface anchoring energies result in complicated configurations such as "spherulites" and "fingers" [70]–[74]. Inside, the cholesteric twists; at the boundary of the configuration, the director adopts a homeotropic orientation in order to match the surrounding matrix, Figure 5.17(a). Usually, this twist is nonsingular (although some types of configurations might contain line [75] or point [76] singularities). If $L/p \sim 1$, a convenient way to analyze both the geometry and energetic stability of configurations is to map the director field onto the sphere S^2 [71]. For example, the double-twisted director field of the finger in Figure 5.17(a) is represented by a lobe on S^2 in Figure 5.17(b). Clearly, the lobe can shrink into a point, say, the north pole of S^2; thus the finger is equivalent to the uniform state $\mathbf{n} = \pm\mathbf{h}$. Any other configuration (even with topological singularities such as

(a)

(b)
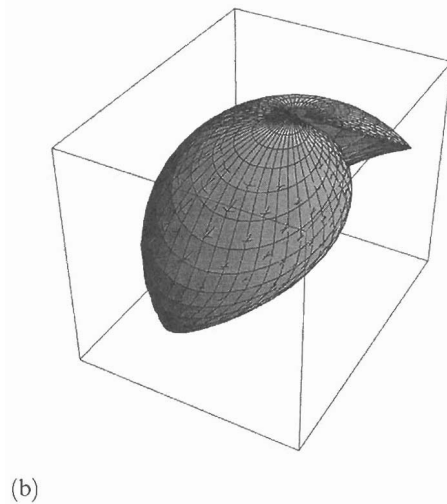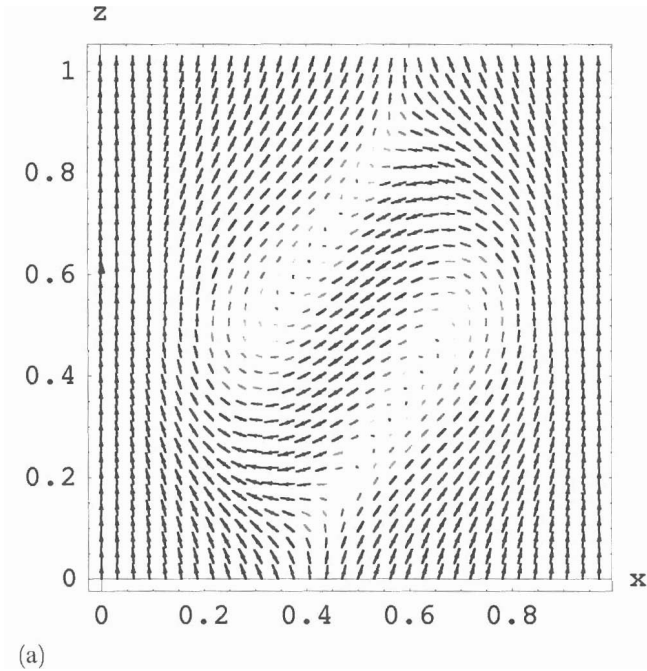
FIGURE 5.17 Computer-generated cross-section of a cholesteric "finger" in a cell with finite surface anchoring and magnetic field: director configuration (a) in the real space and (b) on the sphere S^2 (courtesy S.V. Shiyanovskii).
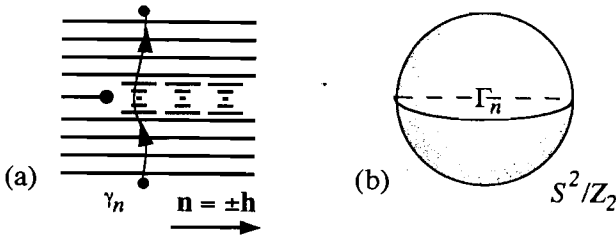
FIGURE 5.18. Twist wall as a planar soliton; director field in (a) the real space and (b) the OP space.

a pair of radial and hyperbolic hedgehogs described by Pirkl et al. [76] for spherulites) that appears from the homeotropic state, should have an image on S^2 that is shrinkable into a point. Of course, when the field is weak, the gain in the twist energy prevents the lobe from shrinking.

Fingers, spherulites, and core structures of the disclinations considered in Section 5.2 have the following common feature: the OP space looks different at different scales. This feature is characteristic of topological solitons that are described by relative homotopy groups [77], [43]. To illustrate the issue, consider first a twisted wall in a nematic cell with tangential boundary conditions subjected to a strong horizontal magnetic field, Figure 5.18(a). The wall might terminate on a disclination line, or, if the line is moved to the sample's boundary on the left, run along the entire sample.

Consider the mapping of the line γ_n threaded through the wall into the OP space. The ends of the line are mapped into antipodal identical points $\mathbf{n} = \pm\mathbf{h}$, while the line γ_n itself is mapped onto the closed contour Γ_n linking these points in the OP space. This contour cannot be contracted to a point by any continuous transformations, as long as the end points are fixed. Therefore, the deformed (but *nonsingular*) configuration is stable. The width of the wall is fixed by the balance of elastic, anchoring, and field energies. Such a structure is called a *topological soliton*. A soliton of the planar type just described can be closed into a loop or terminate at disclinations. Alternatively, a disclination loop (or a pair of disclinations) can nucleate in the plane of the soliton and destroy the wall.

In the general case, the classes of homotopic mappings of the line γ threaded through a planar soliton form the *relative homotopy group* $\pi_1(\mathfrak{R}, \bar{\mathfrak{R}})$, where $\bar{\mathfrak{R}}$ is the OP space far from the core of the soliton, shrunk (as compared to the complete OP space $\mathfrak{R}$) by additional interactions (external field, boundary conditions, etc.). If $\bar{\mathfrak{R}}$ consists of a single point, as in Figure 5.18, $\pi_1(\mathfrak{R}, \bar{\mathfrak{R}})$ coincides with the fundamental group $\pi_1(\mathfrak{R})$ [77], [78].

Just as a disclination in an external field can give rise to a planar soliton, a point defect can give rise to a linear soliton. Linear solitons are described by the classes of mappings of the surface σ crossing the soliton into the OP spaces $\mathfrak{R}$ and $\bar{\mathfrak{R}}$, i.e., by the elements of the second relative group $\pi_2(\mathfrak{R}, \bar{\mathfrak{R}})$.

As already discussed, there are no isolated point defects in the cholesteric phase, $\pi_2(\mathfrak{R} = SO(3)/D_2) = 0$. However, singular point defects can serve as the ends of linear solitons, as in the case of the monopole structure, in which the nonsingular disclinations can be considered as linear solitons.

The most interesting case is presented by the so-called particle solitons. The distribution of the OP in particle-like solitons depends on all three coordinates. They are described by the group $\pi_3(\mathfrak{R}, \bar{\mathfrak{R}})$ of homotopy classes of the mappings of the three-dimensional spherical volume D^3 containing the soliton into the OP space $\mathfrak{R}$. Here the boundary of the spherical volume, the sphere σ, is mapped into the shrunk space $\bar{\mathfrak{R}}$. If $\bar{\mathfrak{R}}$ consists of one point, then the particle-like soliton is described by the group $\pi_3(\mathfrak{R})$. The spherical volume D^3 with all points of its surface σ being equivalent, is homotopic to a three-dimensional sphere S^3 in a four-dimensional space. Thus the elements of $\pi_3(\mathfrak{R})$ are the mappings $S^3 \to \mathfrak{R}$. The special cases $S^3 \to S^2$ and $S^3 \to S^2/Z_2$ are called Hopf mappings, Figure 5.19, and correspond to $\pi_3(S^2) = \pi_3(S^2/Z_2) = \pi_3(SO(3)/D_2) = Z$, where Z is the group of integers; classification for the cholesteric and nematic phases is the same.

In a uniaxial nematic, the particle-like soliton amounts to a director configuration distorted in a region of finite size, outside of which the director field is uniform. As a rule, such solitons are unstable with respect to a decrease in size and subsequent disappearance on scales smaller than the
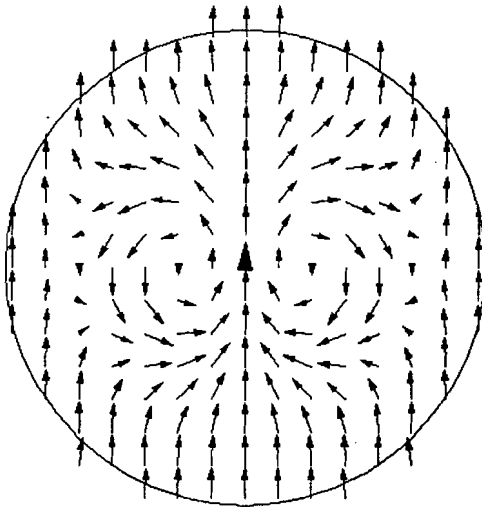
FIGURE 5.19. A nontrivial Hopf texture in a three-dimensional vector field, as seen in the vertical cross-section. The vector field is directed north everywhere outside the sphere and at the origin. The vertical axis is the rotational symmetry axis. When going along any radius from the center to the surface of the sphere, the vector rotates by an angle $2\pi r/R$ around this radius. The length of the arrows is proportional to the length of the vector projection in the XY plane.

coherence length ξ. The decrease in size $L \rightarrow L\mu$ ($\mu < 1$) entails an increase in the elastic-energy density by a factor of $1/\mu^2$ and a decrease in the volume of the soliton by a factor of μ^3, so that the total elastic energy decreases: $F \rightarrow F\mu$. Stabilization of particle-like solitons can be facilitated by an additional interaction, in particular, by helical twisting of the structure [79]. In a weakly twisted cholesteric mixture Bouligand [80], [81] observed two linked disclination rings $k_1 = k_2 = 1$, each of which, by itself, is topologically unstable, whereby all points of the cores of the disclination are mapped into a single point of S^2/Z_2. In going from one ring to the other, the director undergoes a π rotation and one can represent the rings as inverse images of two diametrically opposite points on S^2. Evidently one cannot convert the configuration into a homogeneous state because the rings are linked: upon trying to unlink the rings, they must intersect one another and singularities would arise in the configuration. The degree of linking of the rings, equal in this case to unity, coincides with the Hopf invariant, which is an element of the group $\pi_3(S^2/Z_2) = Z$. The stability of the configuration as a whole is guaranteed by the conservation of the Hopf invariant [81].

5.8   Effects of the Layer Structure

As already mentioned, the layered structure of cholesteric materials imposes certain limitations on the topological classification of defects based on homotopy groups; a more general theory is still lacking. In this section we discuss macroscopic defects such as focal conic domains and oily streaks whose existence depends crucially on the layered character of ordering.

5.8.1   Focal Conic Domains

In the regime $L/p \gg 1$, the elastic theory considers the cholesteric medium as a system of equidistant (and thus parallel) layers and that the curvature distortions are predominant, (5.8). The description of defects such as edge dislocations, oily streaks, and focal conic domains in cholesterics is often based on the results obtained for "simpler" layered medium, namely, the smectic A phase.

The liquid crystal samples are always bounded, so the surface interactions prescribe a certain orientation of the cholesteric layers (most often, the layers align parallel to the bounding surface). Generally, the two requirements (surface orientation and the equidistance of layers) can be satisfied simultaneously only when the layers are bent in a very special manner. As was established by G. Friedel and Grandjean, originally for smectic A phases [82], [83], all the parallel layers should take the shape of "Dupin cyclides." According to Dupin (see, e.g., Darboux [84]), in such a case the two focal surfaces of the layers are degenerate into lines, which are confocal conics (e.g., an ellipse and a hyperbola; or a circle and a straight line; or two pa-
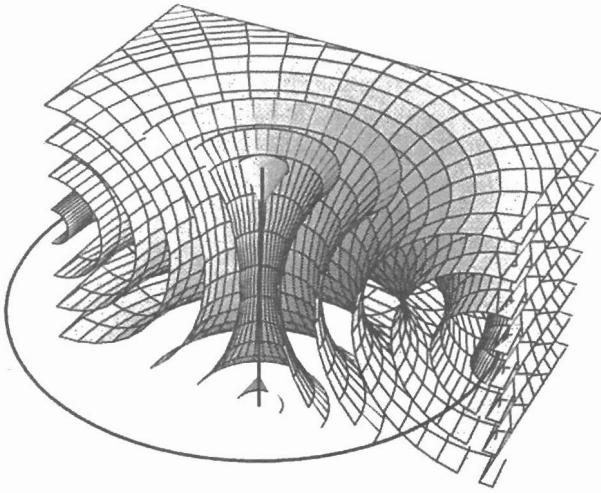
FIGURE 5.20. Focal conic domain with a circular base smoothly embedded in the set of horizontal flat layers. The layers are equidistant everywhere except in the vicinity of the circle and the confocal straight line.

rabolas). The restricted part of space filled with a single family of Dupin cyclides is called a focal conic domain (FCD). Figure 5.20 shows a particular type of toroidal FCD—a circle and a straight line as focal lines (for more details, see [2], [85]). The layered structure inside the FCD exactly matches the planar configuration of the layers outside.

Although the FCDs involve three-dimensional distortions, the elastic energy of an FCD scales linearly with the characteristic size $\sim KL$ (e.g., the size of the elliptical or circular base). When an FCD has its base on the bounding surface, it effectively changes the surface orientation of cholesteric layers: in most experimental situations, the layers are perpendicular to the boundary inside the base, while outside they are parallel. When the surface does not favor the planar orientation of layers, the appearance of FCDs with size $L > L^* = K/(\gamma_\parallel - \gamma_\perp)$ is energetically justified [86]: every domain saves surface energy $(\gamma_\parallel - \gamma_\perp)L^2$ at the expense of elastic energy KL. Recent atomic force examination of FCDs in cholesteric oligomers by Meister et al. [87] reveals smooth matching between layers tilted at the free surface of the sample (inside the FCDs) and flat layers in the bulk that are parallel to the interface (outside the FCDs). Focal conic textures and their transformations under applied electric field, studied for smectic layered systems [88], [89], are used in bistable cholesteric reflective displays [90].

The SMLC cholesterics most frequently present *polygonal textures* with domains of a negative Gaussian curvature. In these domains the focal conditions are not exactly satisfied [91], and unlike the situation in smectics, the cholesteric layers might deviate from the exact geometry of Dupin cyclides

by changing their thickness. In a cholesteric, it is possible to let the pitch vary by a large range at the sole expense of some energy of twist K_2. These polygonal textures are less frequent in biopolymers in solution (DNA, polypeptides, etc.) [45], because the twist energy is accompanied by a considerable bend contribution K_3, caused by the rigidity of the long molecules. We are not aware of any reports on FCDs with a positive Gaussian curvature in the bulk of cholesteric materials (although such domains are documented for lyotropic lamellar phases [92]).

The most rigid cholesteric biopolymers have other types of layer textures, the monopole structures or *Robinson spherulites* discussed in the previous section: the layers are approximately along concentric spheres (positive Gaussian curvature). An extensive study and review of cholesteric spherulites in materials of biological interest can be found in Bouligand and Livolant [57].

5.8.2   Oily Streaks

Oily streaks and liquid crystals were discovered simultaneously. In 1888, F. Reinitzer studied cholesterylbenzoate and noticed elongated "fluid" inclusions in the cholesteric sample [93]. Oily streaks, as FCDs, are common for many lamellar liquid crystals. In a flat cell with layers parallel to the bounding plates, oily streaks appear as long bands that divide the ideal domains of flat layers. Their inner structure is quite complicated and depends on many parameters, most notably on elastic constants [94] (including the saddle-splay elastic constant [95]) and surface anchoring. According to Friedel [83], oily streaks are made of pairs of edge dislocations of (large) opposite Burgers vectors nd, $n'd$, making a total Burgers vector $b = (n - n')d$; here d is the characteristic interlamellae distance, such as the thickness of a smectic A layer or the half-pitch in cholesterics. Each element of the pair is most probably due to the coalescence of small Burger's vector dislocations of the same sign. A large Burgers vector dislocation $b = nd$ can be favoured with respect to small Burgers vectors dislocations $n_i d$, $\sum_i n_i = n$, produced when the sample is formed. The explanation is in the specific model of the dislocation core which is split into two disclinations of opposite signs, Figure 5.21(a); the splitting reduces the total elastic energy of the dislocation [94]. A further feature characteristic of oily streaks is the frequent occurrence of a transversal striation caused either by undulation of the layers or by the formation of FCD chains [95].

The simplest variety of oily streaks is shown in Figure 5.21(b): two parallel $k = \frac{1}{2}$ disclinations with a wall between them. The total Burgers vector is zero, so that the oily streak is topologically trivial and can disappear by pulling the semiround ends together. There is no transversal striation so that the Gaussian curvature is zero everywhere except at the end region (where it is negative).

Since the line tension (the free energy per unit length) of the oily streaks is

(a)

(b)
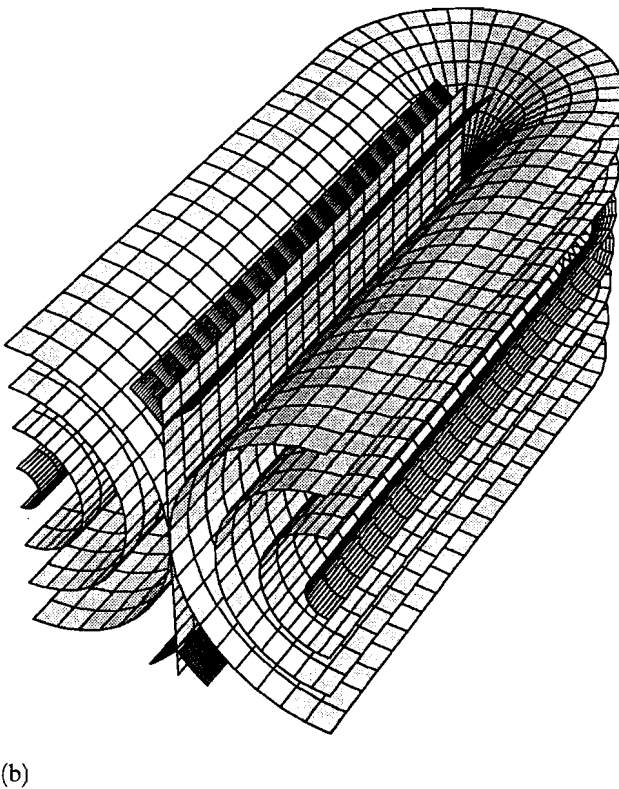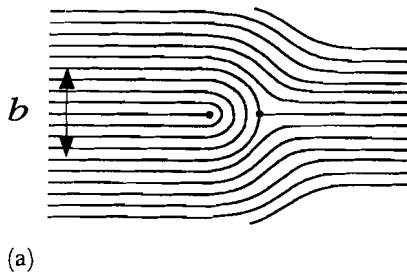
FIGURE 5.21. (a) Splitting of the core of a large Burgers vector dislocation into two disclinations; and (b) an oily streak with a semicircular end in a system of parallel and equidistant layers.

normally positive, their networks coarsen with time. Zapotocky et al. [96] suggested stabilizing the networks of oily streaks by adding micron-size colloidal particles to the cholesteric. The particles gather at the nodes of the network. The stabilized network of connected oily streaks greatly modifies the rheological properties of the system, making it gel-like. In contrast to a
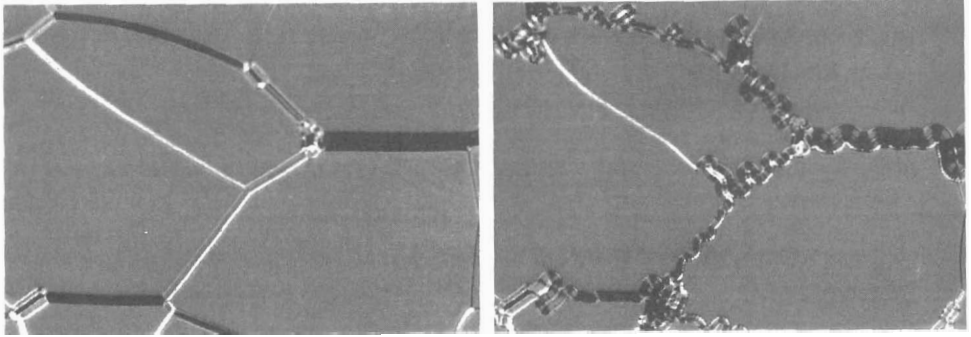
FIGURE 5.22. Network of oily streaks in a cholesteric planar texture. Cell thickness 15 μm, cholesteric pitch 0.48 μm. The oily streaks are (a) straight at zero voltage but (b) buckle when the voltage exceeds some threshold value. The short side of the field of view is 420 μm. The narrow streaks do not buckle while the wide streaks start to buckle at voltages higher than the medium width streaks.

defect-free cholesteric fluid that exhibits liquid-like rheology, the stabilized oily streaks exhibit macroscopic rubber-like elasticity [96].

Usually, the layers within the FCDs and oily streaks, and the layers outside these defects, have different orientation at the sample's boundaries; thus the problems of surface anchoring and the layers' curvature in these defects are strongly connected. To illustrate the relationship, we briefly discuss an electric field instability that manifests itself as a buckling of oily streaks [97]. The electric field changes the line tension of oily streaks and can even drive it negative, in which case the oily streaks buckle and proliferate rather than coarsen.

Figure 5.22(a) shows the network of connected oily streaks in a cholesteric sample when the electric field is absent. The bounding plates of the sample are treated to align the molecules parallel to the plates, so that the field χ is normal to the bounding plates. The edges that separate the uniform domains are oily streaks, provoked by inhomogeneities such as plastic spacers that keep the binding glass plates apart. The width $2a$ of the oily streak is defined by the number of layers that undergo a π turn.

An electric field $\mathbf{E}$ is applied to transparent conducting ITO layers at the bounding plates and is thus normal to the cholesteric layers at the faces. The dielectric anisotropy of the cholesteric material (defined with respect to the helix axis χ) is negative, $\varepsilon_a < 0$, so that the layers tend to reorient along $\mathbf{E}$. One would expect expansion of the oily streaks since the layers are almost parallel to $\mathbf{E}$ inside the oily streak. The experiment, Figure 5.22(b), shows that the expansion takes place as an elongation and buckling of the streaks rather than as their widening: the field drives the line tension of oily streaks negative.

Although the phenomenon is similar in appearance to the buckling of dislocations in Cano wedges [98], [99], it cannot be understood solely as a dielectric response [99] of the cholesteric. The behavior of the oily streaks can be explained only if one adds a specific surface anchoring term with an amplitude $W \sim K/p$ to the standard energy density, comprised of the elastic terms (5.7) and the dielectric term $\sim -\varepsilon_a(\chi \cdot \mathbf{E})^2$.

The anchoring term is caused by tilting the cholesteric layers at the boundaries. The tilt angle increases from 0 outside the streak to $\theta_{\max} = \arctan \xi$ at the vertical middle plane of the streak, see Figure 5.21(b); $\xi = 2a/h$ is the width of the streak renormalized by the cell thickness h. The anchoring penalty increases when $2a$ increases (since $\theta_{\max}$ increases); this increase can be avoided if the oily streak simply elongates, preserving $\theta_{\max} = $ const.

A quantitative analysis [97] with the model of the oily streak depicted in Figure 5.21(b), shows that the elastic, dielectric, and anchoring contributions to the line tension F of the oily streak depend differently on ξ. The elastic term is practically linear with ξ (the slowly changing logarithmic factor $\sim \ln \xi$ can be neglected). The dielectric and anchoring energies scale as ξ^2 when $\xi \ll 1$, but switch to a linear scaling $\sim \xi$ when $\xi \gg 1$. Thus narrow oily streaks are always dominated by the elastic energy and $F > 0$ for any applied voltage. Anchoring takes over at $\xi \gg 1$, so that the line tension of the wide streaks is also positive. For intermediate $\xi \sim 1$, when the field is higher than some threshold value V_{th}, the (negative) dielectric contribution outbalances both the elastic and anchoring terms and drives the line tension negative. The oily streak elongates, preserving the width that corresponds to the minimum of the curve $F(\xi)$ in Figure 5.23, as in the experiment, Figure 5.22(b).
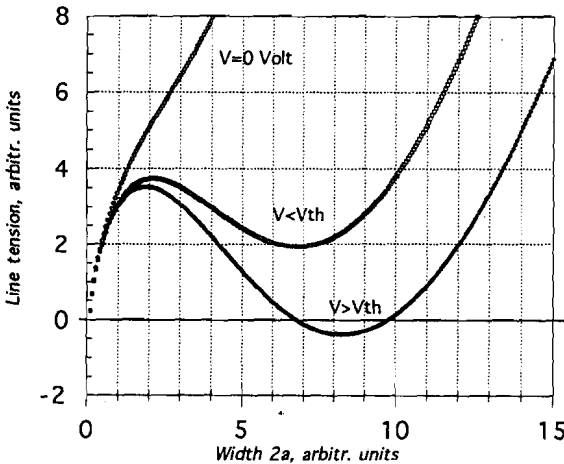
FIGURE 5.23. Line tension of the oily streak as a function of its width for different values of the applied field. Note that at high field only the streaks of intermediate width gain a negative line tension.

Note that a good quantitative agreement between the model and experiment can be obtained only when there is an "intrinsic" contribution $W \sim K/p$ to the anchoring coefficient. It comes from the layered structure of the cholesteric and has no analog in the nematic phase (but has a counterpart in smectics). The estimate $W \sim K/p$ is natural since the number of cholesteric layers crossing the boundary is of the order of θ/p, and each layer has to be distorted (continuously or through dislocations) to accommodate the anchoring direction at the boundary. The energy of these distortions is $\sim K$ per layer. Hence $W \sim K/p$.

5.9   Conclusion

The molecular chirality and tendency of many liquid crystalline phases (even composed of nonchiral molecules) to twist results in spectacular director configurations that often include topological defects and solitons. We covered the very basic properties of deformations related to twisted structures; the considerations were restricted mainly to a uniaxial cholesteric phase in a static regime. Some of the areas where one can expect further exciting progress are listed below.

Although the homotopy theory of classifying defects in condensed media had been developed more that 20 years ago, some theoretical aspects, such as direct inclusion of the large-scale equidistance of layers, can still be advanced. Another field awaiting both theoretical and experimental effort is the hydrodynamics of chiral systems, especially in the presence of defects. Experimentally, some of the predictions of homotopy theory, such as the topological entanglement of disclinations in media with a director's trihedron as the order parameter, remain to be observed. Experimental studies of phases, in which the frustrations between layered (smectic-like) or hexagonal order and twist (or double-twist) deformations are resolved through topological defects, are still in their infancy; major breakthroughs are expected for new liquid crystal materials composed of discotic molecules and polymers.

Many cholesteric structures, especially in the regime $L/p \sim 1$, are too sophisticated to be reconstructed by analytical analysis or by ordinary polarizing microscopy. Development of computer simulations and relatively new experimental techniques, such as confocal microscopy, promises fast progress in the deciphering of chiral configurations. With this background information, the research can further progress into the fascinating areas of new complex materials, in which the liquid crystal serves as the dispersed phase (as in the polymer-dispersed liquid crystals [67], [68]) or as the dispersion medium, as in the example [96] with defect-stabilized cholesteric gels. Defects are topologically inherent in all liquid–crystal disperse systems that have internal surfaces, as discussed in Section 5.6.

One could definitely expect a strengthening of the interplay between cholesteric liquid crystal and biological studies: chirality is one of the most

important features of living species. On a more immediate pragmatic side, studies of defects in cholesteric cells subjected to external fields will advance the design of reflective displays [90] and other devices such as "smart mirrors" [100], or diffraction gratings with electrically controlled periodicity [101].

References

[1] P.G. de Gennes and J. Prost, *The Physics of Liquid Crystals*, 2nd ed., Oxford Science, Clarendon Press, Oxford, 1993.

[2] M. Kleman, *Points, Lines, and Walls*, Wiley, Chichester 1983.

[3] P.M. Chaikin and T.C. Lubensky, *Principles of Condensed Matter Physics*, Cambridge University Press, 1995; T.C. Lubensky, *Solid State Commun.* **102**, 187 (1997).

[4] D.R. Link, G. Natale, R. Shao, J.E. Maclennan, N.A. Clark, E. Körblova, and D.M. Walba, *Science* **278**, 1924 (1997).

[5] G. Heppke and D. Moro, *Science* **279**, 1872 (1998).

[6] M.V. Kurik and O.D. Lavrentovich, *Pis'ma Zh. Eksp. Teor. Fiz.* **35**, 362 (1982), *[JETP Lett.* **35**, 444 (1982)].

[7] L.M. Blinov and V.G. Chigrinov, *Electrooptic Effects in Liquid Crystal Materials*, Springer-Verlag, New York, 1994.

[8] G.P. Crawford and S. Zumer, in: *Liquid Crystals in the Nineties and Beyond* (edited by S. Kumar), p. 331, World Scientific, Singapore, 1995.

[9] R.B. Meyer, in: *Polymer Liquid Crystals* (edited by A. Cifferi et al.), Ch. 6, Academic, New York, 1982.

[10] M. Kleman, *Rep. Prog. Phys.* **52**, 555 (1989).

[11] C. Mauguin, *Bull. Soc. France Mineral* **34**, 71 (1911).

[12] D. Meyerhofer, A. Sussman, and R. Williams, *J. Appl. Phys.* **43**, 3685 (1972).

[13] O.D. Lavrentovich, *Phys. Rev. A* **46**, R722 (1992).

[14] G. Srayer, F. Lonberg, and R.B. Meyer, *Phys. Rev. Lett.* **67**, 1102 (1991); R.B. Meyer, F. Lonberg, V. Taratuta, S. Fraden, S.-D. Lee, and A.J. Hurd, *Faraday Disc. Chem. Soc.* **79**, 125 (1985).

[15] M.J. Press and A.S. Arrott, *Phys. Rev. Lett.* **33**, 403 (1974).

[16] F. Lonberg and R.B. Meyer, *Phys. Rev. Lett.* **55**, 718 (1985).

[17] G.E. Volovik and O.D. Lavrentovich, *Zh. Eksper. Teor. Fiz.* **85**, 1997 (1983), *[Sov. Phys. JETP* **58**, 1159 (1983)].

[18] R.D. Williams, *J. Phys. A: Math. Gen.* **19**, 3211 (1986).

[19] M. Kleman, *J. Phys. (Paris)* **46**, 1193 (1985).

[20] M. Kleman, *J. Phys. Lett.* **46**, L-723 (1985).

[21] D.C. Wright and N.D. Mermin, *Rev. Mod. Phys.* **61**, 385 (1989).

[22] F. Livolant and Y. Bouligand, *Chromosoma* **80**, 97 (1980).

[23] J. Friedel, *Proc. 6th Gen. Conf. Eur. Phys. Soc.* (Prague) (edited by J. Santra and J. Pantoflicék).

[24] M. Kleman, *Phys. Scripta* **T19**, 565 (1987).

[25] F. Livolant and Y. Bouligand, *J. Phys. (Paris)* **47**, 1813 (1986); F. Livolant, A.M. Levelut, J. Doucet, and J.P. Benoit, *Nature* **339**, 724 (1989).

[26] D.H. Van Winkle, M.W. Davidson, W.-X. Chen, and R.L. Rill, *Macromolecules* **23**, 4140 (1990); D.C. Martin and E.L. Thomas, *Phil. Mag. A* **64**, 903 (1991).

[27] R.D. Kamien and D.R. Nelson, *Phys. Rev. Lett.* **74**, 2499 (1995); *Phys. Rev.* **E53**, 650 (1996).

[28] T.C. Lubensky, A.B. Harris, R.D. Kamien, and G. Yan, *Ferroelectrics* **212**, 1 (1998).

[29] P.G. de Gennes, *Solid State Comm.* **10**, 753 (1972).

[30] S.R. Renn and T.C. Lubensky, *Phys. Rev. A* **38**, 2132 (1988); J. Goodby, M.A. Waugh, S.M. Stein, E. Chin, R. Pindak, and J.S. Patel, *Nature* **337**, 449 (1988); T.C. Lubensky and S.R. Renn, *Phys. Rev. A* **41**, 4392 (1990); S.R. Renn, *Phys. Rev. A* **45**, 953 (1992).

[31] B.A. Dubrovin, S.P. Novikov, and A.T. Fomenko, *Sovremennaya Geometriya*, Moscow, Nauka, 760 pp. (1979) (in Russian); [English transl.: *Modern Geometry*, Parts I, II, III, Springer-Verlag, 1985–1992]; A.Yu. Grosberg and A.R. Khokhlov, *Statistical Physics of Macromolecules*, AIP Press, New York, 1994.

[32] F.B. Fuller, *Proc. Nat. Acad. Sci. USA* **68**, 815 (1981).

[33] D. Swigon, B.D. Coleman, and I. Tobias, *Biophys. J.* **74**, 2515 (1998).

[34] *DNA Topology and its Biological Effects* (edited by N. Gozzarelli and J.C. Wang), Cold Spring Harbor Laboratory Press, 1990.

[35] G. Toulouse and M. Kléman, *J. Phys. Lett. (Paris)* **37**, L-149 (1976); M. Kleman, *J. Phys. Lett. (Paris)* **38**, L-199 (1977).

[36] G.E. Volovik and V.P. Mineev, *Pis'ma Zh. Eksp. Teor. Fiz.* **24**, 605 (1976); [*JETP Lett.* **24**, 595 (1976)].

[37] G.E. Volovik and V.P. Mineev, *Zh. Eksper. Teor. Fiz.* **72**, 2256 (1977); [*Sov. Phys. JETP* **45**, 1186 (1977)].

[38] M. Kleman and L. Michel, *Phys. Rev. Lett.* **40**, 1387 (1978).

[39] P. Cladis and M. Kleman, *J. Phys. (Paris)* **33**, 591 (1972).

[40] R.B. Meyer, *Phil. Mag.* **27**, 405 (1973).

[41] J. Friedel and M. Kléman, *Fundamental Aspects of Dislocation Theory* (edited by J.A. Simmons, R. de Wit, and R. Bullough), Special Publication No. 317, Washington, DC: National Bureau of Standards **1**, 715 (1970).

[42] G. Toulouse, *J. Phys. Lett.* **38**, L67 (1977).

[43] V.P. Mineev, *Soviet Scientific Reviews*, Section A: *Physics Reviews*, vol. 2 (edited by I.M. Khalatnikov), p. 173, Harwood Academic, London, 1980.

[44] I.F. Lyuksyutov, *Sov. Phys. JETP* **75**, 358 (1978).

[45] F. Livolant, *J. Phys.* **47**, 1605 (1986).

[46] Y. Bouligand and M. Kléman, *J. Phys. France* **31**, 1041 (1970).

[47] P.E. Cladis and M. Kléman, *Mol. Cryst. Liq. Cryst.* **16**, 1 (1972).

[48] A. Saupe, *Mol. Cryst. Liq. Cryst.* **21**, 211 (1973).

[49] R. Meister, H. Dumoulin, M.-A. Hallé, and P. Pieranski, *J. Phys. II France* **6**, 827 (1996).

[50] V. Poenary and G. Toulouse, *J. Phys. (Paris)* **38**, 887 (1977).

[51] M.I. Monastyrsky and V.S. Retakh, *Commun. Math. Phys.* **103**, 445 (1986).

[52] K. Janich and H.R. Trebin, *Physique des Défauts/Physics of Defects* (edited by R. Balian et al.), p. 421, Les Houches, Session XXXV, 1980; North-Holland, Amsterdam, 1981.

[53] M. Kleman, *Phil. Mag.* **27**, 1057 (1973).

[54] C. Robinson, *Trans. Faraday Soc.* **52**, 571 (1956); C. Robinson, J.C. Ward, and R.B. Beevers, *Discuss. Faraday Soc.* **25**, 29 (1958).

[55] M.V. Kurik and O.D. Lavrentovich, *Mol. Cryst. Liq. Cryst. (Lett.)* **72**, 239 (1982).

[56] M.V. Kurik and O.D. Lavrentovich, *Zh. Eksper. Teor. Fiz.* **85**, 511 (1983); [*Sov. Phys. JETP* **58**, 299 (1983)].

[57] Y. Bouligand and F. Livolant, *J. Phys. (Paris)* **45**, 1899 (1984).

[58] J. Bezic and S. Zumer, *Liq. Cryst.* **11**, 593 (1992).

[59] F. Xu and P.P. Crooker, *Phys. Rev.* **E56**, 6853 (1997); R.R. Swisher, H. Hue, and P.P. Crooker, *Liq. Cryst.* **26**, 57 (1999).

[60] P.A.M. Dirac, *Proc. Roy. Soc. London, A* **133**, 60 (1931).

[61] G.E. Volovik, *Pis'ma Zh. Eksp. Teor. Fiz.* **28**, 65 (1978); [*JETP Lett.* **28**, 59 (1978)].

[62] N.D. Mermin, in: *Quantum Fluids and Solids* (edited by S.B. Trickey, E.D. Adams, and J.F. Dufty), p. 3, Plenum Press, New York, 1977, *Boojums All the Way Through*, Cambridge University Press, New York, 1990, 310 pp.

[63] P.P. Crooker and D.K. Yang, *Appl. Phys. Lett.* **57**, 2529 (1990).

[64] O.D. Lavrentovich and Yu.A. Nastishin, *Pis'ma Zh. ETP* **40**, 242 (1984); [*Sov. Phys. JETP Lett.* **40**, 1015 (1984).

[65] O.D. Lavrentovich, Yu.A. Nastishin, V.I. Kulishov, Yu.S. Narkevich, A.S. Tolochko, and S.V. Shiyanovskii, *Europhys. Lett.* **13**, 313 (1990).

[66] H.-S. Kitzerow, *Liq. Cryst.* **16**, 1 (1994).

[67] P.S. Drzaic, *Liquid Crystal Dispersions*, World Scientific, Singapore, 1995, 430 pp.

[68] O.D. Lavrentovich, *Liq. Cryst.* **24**, 117 (1998).

[69] P. Poulin, H. Stark, T.C. Lubensky, and D.A. Weitz, *Science* **275**, 1770 (1997).

[70] M. Brehm, H. Finkelmann, and H. Stegemeyer, *Ber. Bunsen-Ges. Phys. Chem.* **78**, 883 (1974).

[71] F. Lequeux, P. Oswald, and J. Bechhoefer, *Phys. Rev.* **A40**, 3974 (1989); F. Lequeux, *J. Phys. France* **49**, 967 (1988).

[72] J. Baudry, S. Pirkl, and P. Oswald, *Phys. Rev.* **E57**, 3038 (1998).

[73] L. Gil and G.M. Gilli, *Phys. Rev. Lett.* **80**, 5742 (1998).

[74] T. Nagaya, Y. Hikita, H. Orihara, and Y. Ishibashi, *J. Phys. Soc. Jap.* **67**, 2546 (1998).

[75] P. Ribière, P. Oswald, and S. Pirkl, *J. Phys. II France* **4**, 127 (1994).

[76] S. Pirkl, P. Ribière, and P. Oswald, *Liq. Cryst.* **13**, 413 (1993).

[77] V.P. Mineyev and G.E. Volovik, *Phys. Rev. B* **18**, 3197 (1978).

[78] R. Kutka, H.-R. Trebin, and M. Kiemes, *J. Phys. France* **50**, 861 (1989).

[79] R.D. Pisarski and D.L. Stein, *J. Phys. (Paris)* **41**, 345 (1980).

[80] Y. Bouligand, *J. Phys. France* **35**, 959 (1974).

[81] Y. Bouligand, B. Derrida, V. Poenaru, Y. Pomeau, and G. Toulouse, *J. Phys. France* **39**, 863 (1978).

[82] G. Friedel and F. Grandjean, *Bull. Soc. Franc. Minér.* **33**, 192 and 409 (1910); *C. R. Hebd. Séan. Acad. Sci.* **151**, 762 (1910).

[83] G. Friedel, *Ann. Phys. (Paris)* **18**, 237 (1922).

[84] G. Darboux, *Théorie Générale des Surfaces*, republished by Chelsea, New York, 1954.

[85] P. Boltenhagen, M. Kléman, and O.D. Lavrentovich, in: *Soft Order in Physical Systems* (edited by Y. Rabin and R. Bruinsma), p. 5, Plenum Press, New York, 1994.

[86] O.D. Lavrentovich, *Zh. Eksp. Teor. Fiz.* **91**, 1666 (1986); [*Sov. Phys. JETP* **64**, 984 (1986)].

[87] R. Meister, M.-A. Hallé, H. Dumoulin, and P. Pieranski, *Phys. Rev. E* **54**, 3771 (1996).

[88] O.D. Lavrentovich, M. Kléman, and V.M. Pergamenschik, *J. Phys. II (Paris)* **4**, 377 (1994).

[89] Z. Li and O.D. Lavrentovich, *Phys. Rev. Lett.* **73**, 280 (1994).

[90] D.K. Yang and J.W. Doane, *SID Technical Papers Digest* **23**, 759 (1992).

[91] Y. Bouligand, *J. Phys. (Paris)* **33**, 715 (1972).

[92] P. Boltenhagen, O.D. Lavrentovich, and M. Kléman, *Phys. Rev. A* **46**, R1743 (1992); P. Boltenhagen, M. Kléman, and O.D. Lavrentovich, *C. R. Acad. Sci. Paris* **315**, Série II, 931 (1992).

[93] F. Reinitzer, *Monatsh. Chem.* **9**, 421 (1888).

[94] M. Kleman and C.E. Williams, *Phil. Mag.* **28**, 725 (1973); *J. Phys. Lett.* **35**, L-49 (1974).

[95] P. Boltenhagen, O.D. Lavrentovich, and M. Kléman, *J. Phys. II France* **1**, 1233 (1991).

[96] M. Zapotocky, L. Ramos, P. Poulin, T.C. Lubensky, and D.A. Weitz, *Science* **283**, 209 (1999).

[97] O.D. Lavrentovich and D.-K. Yang, *Phys. Rev.* **E57**, R6269 (1998).

[98] Orsay liquid crystal group, *Phys. Lett. A* **28**, 687 (1969).

[99] M. Kleman and J. Friedel, *J. Phys. (France)* **30**, C4-43 (1969).

[100] R.B. Meyer, F. Lonberg, and C.-C. Chang, *Mol. Cryst. Liq. Cryst.* **288**, 47 (1996).

[101] D. Subacius, S.V. Shiyanovskii, Ph. Bos, and O.D. Lavrentovich, *Appl. Phys. Lett.* **71**, 3323 (1997).